EUROPEAN ORGANIZATION FOR NUCLEAR RESEARCH

SL / Note 2001-046
CERN / INTC 2001-038
INTC-O-007

10 December 2001

Study of the Background in the Measuring Station at the n_TOF Facility at CERN: Sources and Solutions

The n_TOF Collaboration‡

Abstract

A background roughly two orders of magnitude higher than tolerable was found in the n_TOF facility at CERN during the first measurements [1]. This note describes a series of additional measurements performed in the n_TOF experimental area to study the origin and the characteristics of the background. The program of these measurements was determined taking into account the results from the simulations carried out by the EET group [2].

A first phase of measurements confirmed the results of the simulations, namely that the dominant source of background was due to neutrons generated by negative muon capture. Actions to reduce the background were taken according to the results from both measurements and simulations. An iron shielding wall 3.2 m thick was then placed in between the sweeping magnet and the second collimator, with the purpose of stopping most of the muons.

In a second phase of measurements, results showed that the additional shielding reduced the main component of the background by about a factor of 30.

‡ABBONDANNO U.[18], AERTS G.[8], ANDRIAMONJE S.[8], ANDRZEJEWSKI J.[22], ANGELOPOULOS A.[10], ASSIMAKOPOULOS P.[13], BACRI C-O.[6], BADUREK G.[1], BERTHOUMIEUX E.[8], BAUMANN P.[7], BEER H.[9], BENLLIURE J.[30], BERTHIER B.[6], BONDARENKO I.[24], BORCEA C.[4], BOS A.J.J.[34], BOSCOLO-MARCHI E.[17], BUSTREO N.[17], CALVINO F.[31], CANO-OTT D.[26], CAPOTE R.[29], CARLSON P.[32], CHARPAK G.[4], CHAUVIN N.[6], CENNINI P.[4], CHEPEL V.[23], COLONNA N.[18], CORTES G.[31], CORTINA D.[30], CORVI F.[21], CUSMANO A.[19], DABABNEH S.[9], DAHLFORS M.[4], DAMIANOGLOU D.[14], DAVID S.[6], DIMOVASILI E.[10], DOMINGO C.[27], DOROSHENKO A.[25], DURAN ESCRIBANO I.[30], ELEFTHERIADIS C.[14], EMBID M.[26], FERRANT L.[6], FERRARI A.[4], FERREIRA–MARQUES R.[23], FRAIS–KOELBL H.[3], FURMAN W.[24], FURSOV B.[25], GARZON J.A.[30], GIOMATARIS I.[8], GLEDENOV Y.[24], GONZALEZ–ROMERO E.[26], GOVERDOVSKI A.[25], GRAMEGNA F.[17], GRIESMAYER E.[3], GUNSING F.[8], HAEFNER P.[4], HAIGHT R.[35], HEIL M.[9], HERRERA-MARTINEZ A.[4], HOLLANDER P.[34], IOANNIDES K.G.[13], IOANNOU P.[10], ISAEV S.[25], JERICHA E.[1], KADI Y.[4], KAEPPELER F.[9], KARADIMOS D.[15], KARAMANIS D.[13], KAYUKOV A.[24], KAZAKOV L.[25], KELIC A.[7], KETLEROV V.[25], KITIS G.[14], KOEHLER P.E.[36]., KOPACH Y.[24], KOSSIONIDES E.[12], KROSHKINA I.[25], LACOSTE V.[4], LAMBOUDIS C.[14], LEEB H.[1], LEPRETRE A.[8], LOPES M.[23], LOZANO M.[29], MARRONE S.[18], MARTINEZ-VAL J. M.[28], MASTINU P.[17], MENGONI A.[16], MEUNIER R.[5], MEZENTSEVA J.[24], MILAZZO P.[19], MINGUEZ E.[28], MITROFANOV V.[25], MOREAU C.[6], MULLER A.[4], NICOLIS N.[13], NIKOLENKO V.[24], OBERHUMMER H.[1], PAKOU A.[13], PANCIN J.[8], PAPADOPOULOS K.[11], PAPAEVANGELOU T.[14], PARADELA C.[30], PARADELIS T.[12], PAVLIK A.[2], PAVLOPOULOS P.[13,33,*], PEREZ-PARRA A.[26], PERRIALE L.[17], PERLADO J. M.[28], PESKOV V.[32], PIKSAIKIN V.[25], PLAG R.[9], PLOMPEN A.[21], PLUKIS A.[8], POCH A.[31], POLICARPO A.[23], POPOV A.[24], POPOV Y.P.[24], PRETEL C.[31], QUESADA J.M.[29], RADERMACHER E.[4], RAPP W.[9], RAUSCHER T.[33], REIFARTH R.[9], REJMUND F.[6], RUBBIA C.[20], RUDOLF G.[7], RULLHUSEN P.[21], SAKELLIOU L.[10], SALDANA F.[4], SAMYLIN B.[25], SAVVIDIS I.[14], SAVVIDIS S.[15], SEDYSHEV P.[24], STEPHAN C.[6], SZALANSKI P.[22], TAGLIENTE G.[18], TAIN J.L.[27], TAPIA C.[31], TASSAN–GOT L.[6], TERCHYCHNYI R.[25], TSABARIS C.[11], TSANGAS N.[15], van EIJK C.W.E.[34], VANNINI G.[18], VENTURA A.[16], VILLAMARIN A.[26], VLACHOUDIS V.[4], VLASTOU R.[11], VOINOV A.[24], VOSS F.[9], WENDLER H.[4,**], WIESCHER M.[37], WISSHAK K.[9], ZANINI L.[4], ZEINALOV S.[25], ZHURAVLEV B.[25]

* *Spokesperson*
** *Technical Coordinator*

1. Atominstitut der Österreichischen Universitäten, Technische Universität Wien, Austria
2. Institut für Isotopenforschung und Kernphysik, Universität Wien, Austria
3. Fachhochschule Wr. Neustadt, Wien, Austria
4. CERN, Geneva, Switzerland
5. Centre National de la Recherche Scientifique/IN2P3, CSNSM, Orsay, France
6. Centre National de la Recherche Scientifique/IN2P3, IPN, Orsay, France
7. Centre National de la Recherche Scientifique/IN2P3, IreS, Strasbourg, France
8. Commissariat à l'Energie Atomique/DSM, Gif-sur-Yvette, France
9. Forschungszentrum Karlsruhe GmbH (FZK), Institut für Kernphysik, Germany
10. Astro-Particle Consortium, Nuclear Physics Lab., University of Athens, Greece
11. Astro-Particle Consortium, Nuclear Physics Dep., Technical University of Athens, Greece
12. Astro-Particle Consortium, Nuclear Physics Institute, NCSR "Demokritos", Athens, Greece
13. Astro-Particle Consortium, Nuclear Physics Lab., University of Ioannina, Greece
14. Astro-Particle Consortium, Nuclear Physics Lab., University of Thessaloniki, Greece
15. Astro-Particle Consortium, Nuclear Physics Dep., University of Thrace, Greece
16. ENEA, Applied Physics Division, Bologna, Italy
17. Laboratori Nazionali di Legnaro, Italy
18. Instituto Nazionale di Fisica Nucleare-Bari, Italy
19. Instituto Nazionale di Fisica Nucleare-Trieste, Italy
20. Università degli Studi Pavia, Pavia, Italy
21. JRC-EC, IRMM, Geel, Belgium
22. University of Lodz, Lodz, Poland
23. Laboratorio de Instrumentacao e Phisica Experimental de Particulas,LIP-Coimbra & Departamento de Fisica da Universidade de Coimbra, Portugal
24. Joint Institute for Nuclear Research, Frank Laboratory of Neutron Physics, Dubna, Russia
25. Institute of Physics and Power Engineering, Kaluga region, Obninsk, Russia
26. Centro de Investigaciones Energeticas Medioambientales y Technologicas, Madrid, Spain
27. Consejo Superior de Investigaciones Cientificas – University of Valencia, Spain
28. Universidad Politecnica de Madrid, Spain
29. Universidad de Sevilla, Spain
30. Universidade de Santiago de Compostela, Spain
31. Universitat Politecnica de Catalunya, Barcelona, Spain
32. Kungliga Tekniska Hogskolan, Physics Department, Stockholm, Sweden
33. Department of Physics and Astronomy, University of Basel, Basel, Switzerland
34. Delft University of Technology, Interfaculty Reactor Institute, Delft, The Netherlands
35. Los Alamos National Laboratory, New Mexico, USA
36. Oak Ridge National Laboratory, Physics Division, Oak Ridge, USA
37. University of Notre Dame, Notre Dame, USA

1. INTRODUCTION

The measurements performed at the n_TOF facility until June 2001 [1] showed that the background for capture measurements is about two orders of magnitude larger than tolerable, making it impossible to pursue the foreseen experimental program. Some features of this background emerged from the measurements, out of which the most important are the following:

- a strong asymmetry, with a higher background on the right side of the experimental area, looking from the target, measured with TLD detectors, sensitive to energy deposition;
- the presence of two main components of the background: a *fast* component, coming with the γ flash or a few microseconds later; and a *slow* component, coming at later times, up to 15 ms;
- an intense prompt pulse present also outside the beam.

The fast component was associated with muons produced following the spallation reactions in the n_TOF target and the subsequent decay of pions and kaons.

However, from these measurements the origin of the slow component of the background was not clear, although it was attributed to fast neutrons: one of the possible origins was that this background was mainly due to fast neutrons originating in the target zone, traveling through the tunnel (outside the beam tube) and arriving in the experimental area, being heavily attenuated by several shielding walls but possibly not enough. Clearly, this hypothesis needed to be tested.

An extensive study of the background was then undertaken consisting of both simulations and measurements. The results from the simulations have been reported in Ref. [2]. The simulations confirmed that the fast background component was due to muons, and revealed that the origin of the slow component was due to the negative muons and not to fast neutrons from the spallation source.

According to the simulations, the strongest contribution to the neutron background observed in the experimental area originates from muons produced after the interaction of the proton beam in the n_TOF target. Neutrons are produced next to the experimental area from muonic capture in the surrounding materials and walls. On the contrary, the simulations indicate that the background due to fast neutrons coming from the target area is not a relevant contribution. From the results of these simulations a possible solution was to reduce strongly the muon flux and therefore the neutron background, by mounting an iron shielding, about 3 m thick, between the sweeping magnet and the second collimator.

In this report we describe the experimental measurements of the background in the n_TOF experimental area. The experimental program was divided into three steps:

- *i)* a **first phase** of measurements to characterize the background in the experimental hall and to test the different hypotheses on the origin of the background;
- *ii*) intervention in the n_TOF tunnel to install the shielding as suggested by the results from the first phase;
- *iii*) a **second phase** of measurements to measure the background reduction in the experimental hall.

2. THE EXPERIMENTAL PROGRAM

The **first phase** of measurements lasted from September 17 to October 10. After performing the reference measurements *(measurement #0)*, i.e. measurements with the facility in the same conditions as in April-June 2001, a 40 cm thick wall was mounted directly behind the 3.2 m wall separating the experimental area from the second collimator region (*measurement #1)*. The wall consisted of stacks of normal and barytic concrete blocks (see Figure 1). From this measurement a strong indication about the mechanism of background production was expected. The aim of the test was to discriminate between the two models of background production, since the attenuation of the background is expected to be different for neutrons and muons. For fast neutrons coming from the target the attenuation with a 40 cm wall is expected to be of about a factor 3, while for muons it is expected to be much lower.

Figure 1. The 40 cm thick concrete wall mounted between the second collimator region and the experimental area.

Afterwards, a beam stopper was placed inside the first collimator *(measurement #2)*. The stopper consisted of iron cylinders 10.5 cm in diameter, and of a total length of about 110 cm. The purpose was to measure the variation of the background inside the experimental area by removing any contribution from the neutron beam.

After the first phase, the measurement program was stopped in order to mount a shielding as suggested by the simulations. The shielding consisted of a 3.2 m thick iron wall placed in the n_TOF tunnel, in between the magnet and the second collimator (Figure 2). Ideally, this wall should have been made entirely of iron, and should have closed the full section of the tunnel. For technical reasons, the wall closed only the right-hand section of the tunnel, covering an area of about 2.8 m × 3.4 m, and the base was made of concrete. Moreover, the density of the iron bricks was lower than the density used in the calculations.

The wall was built in two parts, each 1.6 m long, placed at a distance of 1 m from each other (Fig. 2c). The first part was placed at a distance of 10 m from the magnet. As shown in Figure 2b, an area of about 3% of the right-hand side of the tunnel is not shielded.

The **second phase** of measurements started on October 24 and lasted until November 5. Measurements were taken first with the beam stopper still in position (*measurement #3*), without the 40 cm wall. Then the beam stopper was removed from the first collimator (*measurement #4*). Finally, the 40 cm wall was reinstalled (*measurement #5*).

Some measurements were performed with C and Au samples to estimate the sample-related background, but also to measure the capture resonance spectra with the C_6D_6 counters.

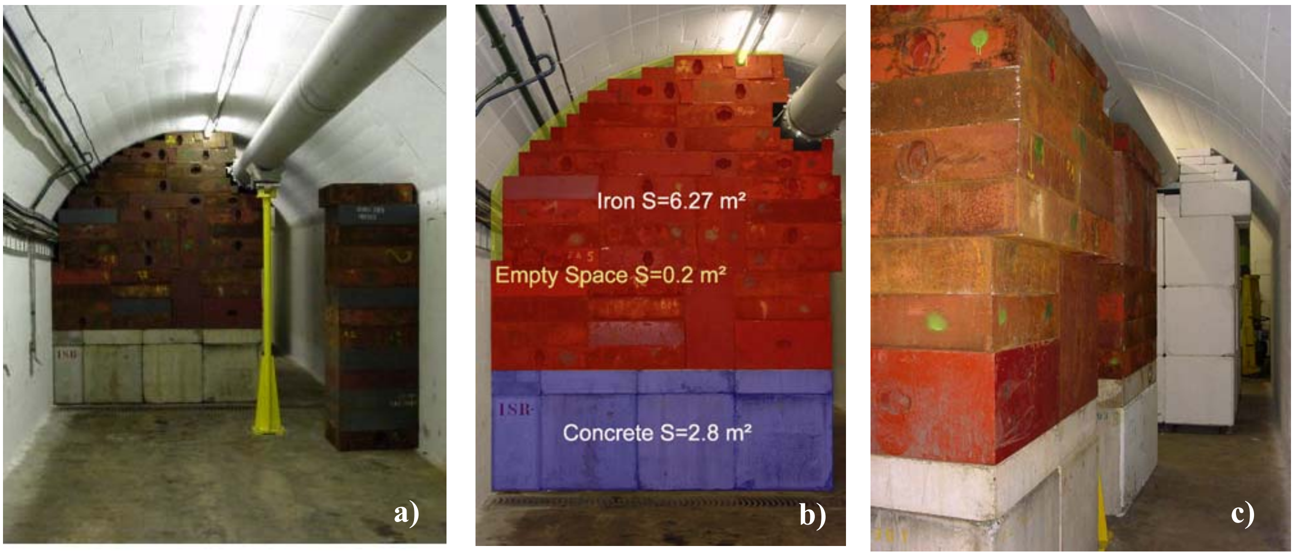

Figure 2. The 3.2 m long iron wall mounted in the n_TOF tunnel 10 m after the sweeping magnet. a): front view from the second collimator. b): front view showing the area of concrete, iron and the empty space. c): side view.

3. THE FIRST PHASE OF MEASUREMENTS

Different types of detectors have been used for neutron and γ-ray detection:

- one ^{3}He proportional counter for neutron detection.
- two C_6D_6 liquid scintillators, and one high-purity germanium detector, from CEA/Saclay, for measurement of γ rays.

The data acquisition implemented for the commissioning of the facility and described in Ref. [3] was used for all detectors.

Measurements were taken with the detectors placed in different positions, as shown in Figure 3. Figure 4 shows one configuration with the two C_6D_6 mounted in positions 1 and fixed, and the ^{3}He placed in position 4.

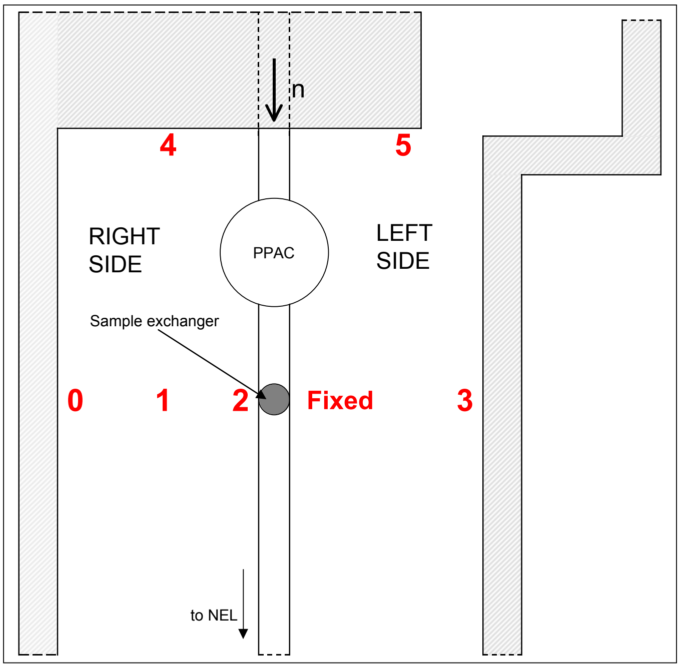

Figure 3. Schematic view of the n_TOF measuring station. The positions in which the detectors were placed are indicated.

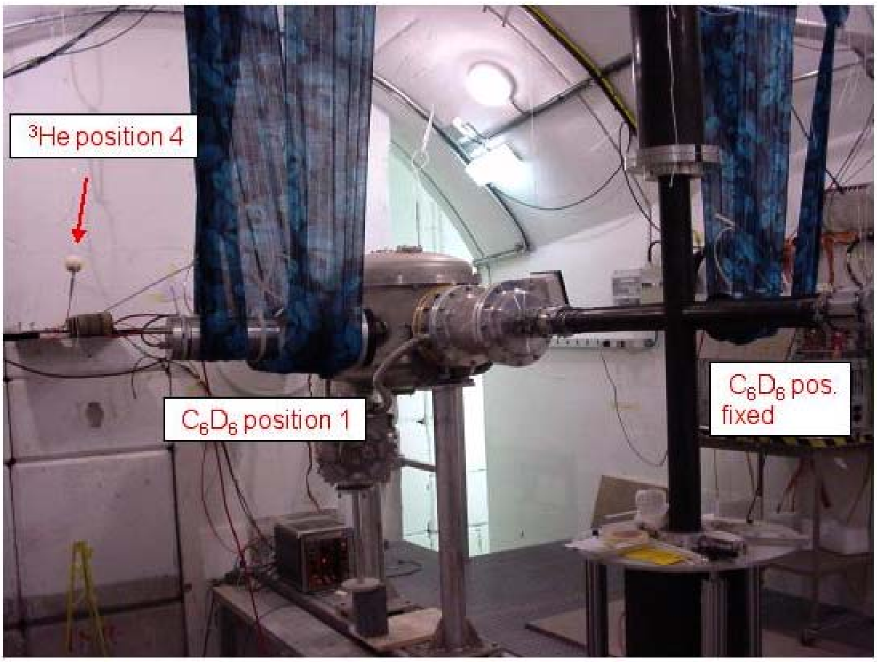

Figure 4. View of the experimental area with two C_6D_6 detectors mounted in position 1 and fixed. The ^{3}He detector with the small polyethylene sphere is mounted in position 4.

3.1 NEUTRON MEASUREMENTS

For neutron measurements a ^{3}He detector (SP9 Centronix) provided by INFN/University of Milano, was used. The detector had a spherical shape (30 mm diameter), containing a mixture of ^{3}He (2 atm pressure) and Kr (1 atm). The detector was mostly used inside spheres of polyethylene of different diameter, 81 mm and 233 mm, being therefore sensitive to different neutron energy regions, as shown in Figure 5. Measurements with a 1 mm thick layer of cadmium covering the 81 mm sphere to cut the thermal neutrons were also performed.

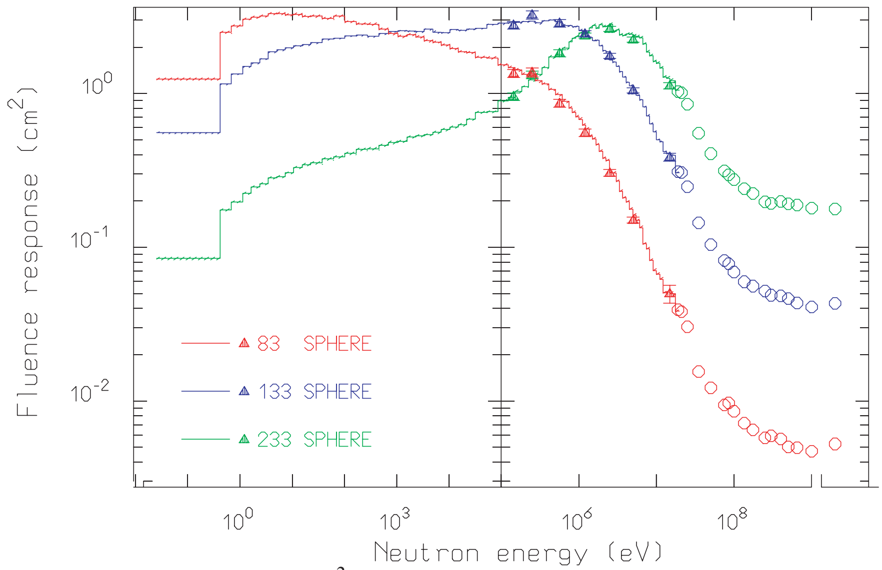

Figure 5. Sensitivity of the ^{3}He detector in different configurations. The triangles refer to calibration measurements performed at the PTB in Germany, the lines and the open circles are from simulations. The sensitivity for the detector with the 81 mm polyethylene sphere is very close to the one with 83 mm shown.

The sensitivity for the ^{3}He detector with the 81 mm polyethylene sphere goes from thermal neutrons up to a few MeV. The addition of a cadmium layer cuts the thermal neutrons. For the configuration with the 233 mm polyethylene sphere the sensitivity is from about 500 keV up to some tens of MeV. The bare ^{3}He counter, not shown in the figure, is sensitive only to thermal neutrons.

The time information from the ^{3}He detector was obtained by triggering on the trailing edge of the pulse. The related jitter, combined with the time spread caused by the thermalization process, gives a time resolution of about 5 μs.

The measurements were taken with the ^{3}He detector in different configurations and placed mainly in four different positions (Figure 3):

- two positions near the wall separating the hall from the n_TOF tunnel, at the right and at the left with respect to the beam line (position 4 and position 5, respectively);
- two positions approximately in the center of the room, one in the right and one in the left side (positions 1 and 3, respectively).

Throughout this paper the number of counts are normalized to the standard proton intensity of 7×10^{12} protons and the γ flash is subtracted.

The total number of counts for measurements in different configurations and positions is given in Table 1. The results were obtained for the reference measurement, then after the 40 cm wall installation, and finally with the beam stopper plugged in the first collimator. The thermal contribution is estimated after correction for the relative efficiencies at thermal and high energy.

Table 1. Counts per 7×10^{12} protons with the ^{3}He detector in different positions and configurations during the measurements #0, #1 and #2. The thermal contribution is calculated by subtracting "Small poly +Cd" from "Small poly", and correcting for the relative efficiency of the detector at thermal and high energy. The statistical uncertainties on the detector counts are indicated.

Position #	Small poly	Small poly + Cd	Thermal Contribution (%)	Big poly
MEASUREMENT #0				
1	5.428 ± 0.078	2.894 ± 0.043	57.4	
2	5.457 ± 0.079	3.021 ± 0.048	55.3	
3	5.026 ± 0.065	2.808 ± 0.037	54.8	
4	8.042 ± 0.055	4.373 ± 0.066	56.0	7.94 ± 0.11
5	5.150 ± 0.081	3.049 ± 0.048	51.4	2.887± 0.044
MEASUREMENT #1: 40 cm WALL				
4	6.882 ± 0.081	4.052 ± 0.051	51.8	
5	4.428 ± 0.084	2.555 ± 0.055	53.0	2.59 ± 0.12
MEASUREMENT #2: 40 cm WALL + BEAM STOPPER				
4	6.365 ± 0.083	3.824 ± 0.076	50.5	
5	4.156 ± 0.070			

3.1.1 Reference Measurements: Contribution of Different Energy Domains

The time spectra obtained with the ^{3}He counter in position 4, with the 81 mm polyethylene sphere with and without the cadmium cover are shown in Figure 6. With the cadmium layer the thermal neutrons are removed and therefore the difference between the two configurations gives the counts due to thermal neutrons only.

As shown in the figure, thermal neutrons correspond to detection times longer than ≈0.25 ms. In terms of neutron time-of-flight, this background has an effect on neutrons with energies up to the keV region. The fraction of thermal neutrons detected is about 45% of all detected neutrons, without correction for the efficiency, or about 55% with efficiency correction (Table 1).

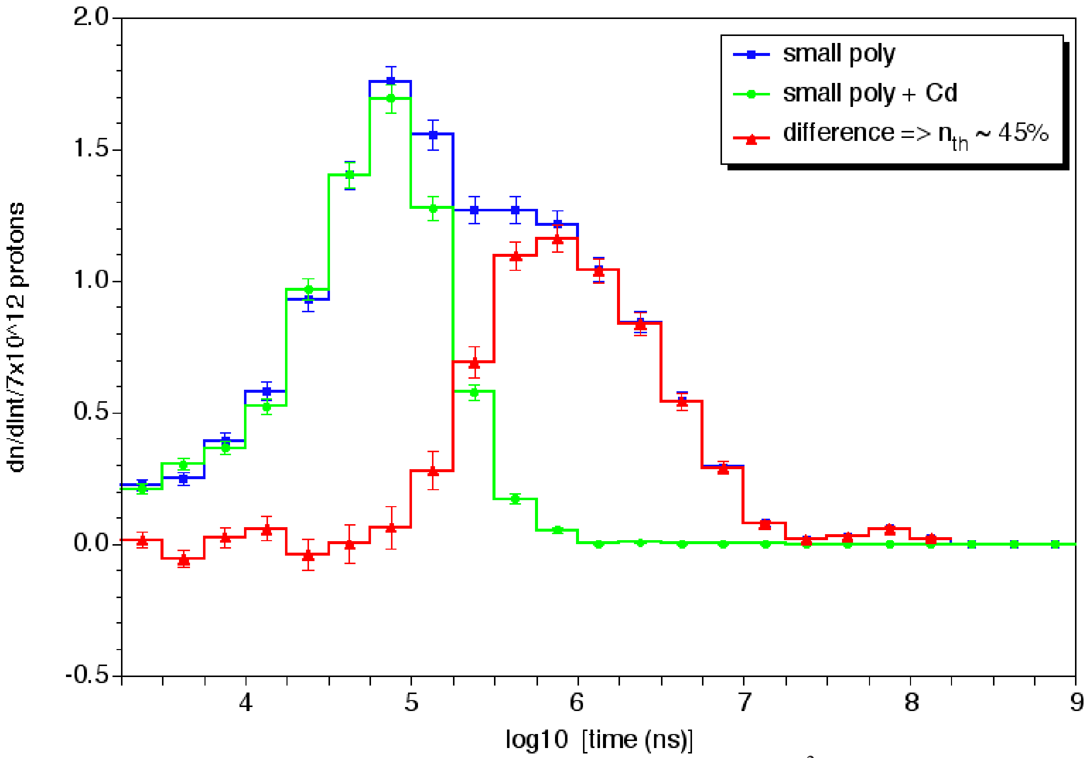

Figure 6. Time spectra measured in position 4 with the ^{3}He with the small polyethylene sphere (blue line), and with the additional Cd layer (green line). The red line, the difference of the two curves, gives the contribution of the thermal neutrons.

3.1.2 Reference Measurements: Left-Right Asymmetry

Measurements were performed with the detector in two positions at the right side of the experimental hall (positions 4 and 1) and in two positions at the left side (positions 5 and 3).

From Table 1 the following values for the left-right asymmetry in the reference measurements near the wall (positions 5 relative to position 4) are obtained: 36% with the small polyethylene sphere, 30% with the additional Cd layer, 42% for the thermal part. These numbers decrease to 8%, 3% and 13%, respectively, when the asymmetry is measured in position 3 relative to position 1. Therefore, the asymmetry near the wall is much more pronounced than in the center of the room. There is a greater asymmetry for fast neutrons, 64% more counts in position 4 than in position 5 with the big polyethylene sphere. These results are in agreement with the expectations from the simulations [2]. In fact, according to the simulations, neutrons are produced mainly by muons interacting with the material surrounding the experimental area. The "hot spot" for neutron production is on the wall at the right side, looking from the target. Therefore, a left-right asymmetry is expected near this wall; since the produced background neutrons diffuse in the experimental hall, this effect is expected to gradually wash out in the center of the room.

The left plot of Figure 7 shows the neutron time spectra taken with the detector surrounded by the small polyethylene sphere, in positions 4 and 5. The flux given for times shorter than 3.2 μs is not considered, as this time domain is affected by the γ flash. The blue curve in the left plot is the difference between positions 4 and 5. On the right-side plots of Figure 7 the differences between the detector with small polyethylene sphere and the detector with small polyethylene sphere + Cd, that is, the contribution of the thermal neutrons, is shown. Again, the blue curve is the difference of the curves in position 4 and 5, and shows that for thermal neutrons at times longer than 10 ms there is no asymmetry. Since this part is beam related, as it will be demonstrated in section 3.1.4, no asymmetry exists for the thermal neutron beam-related background.

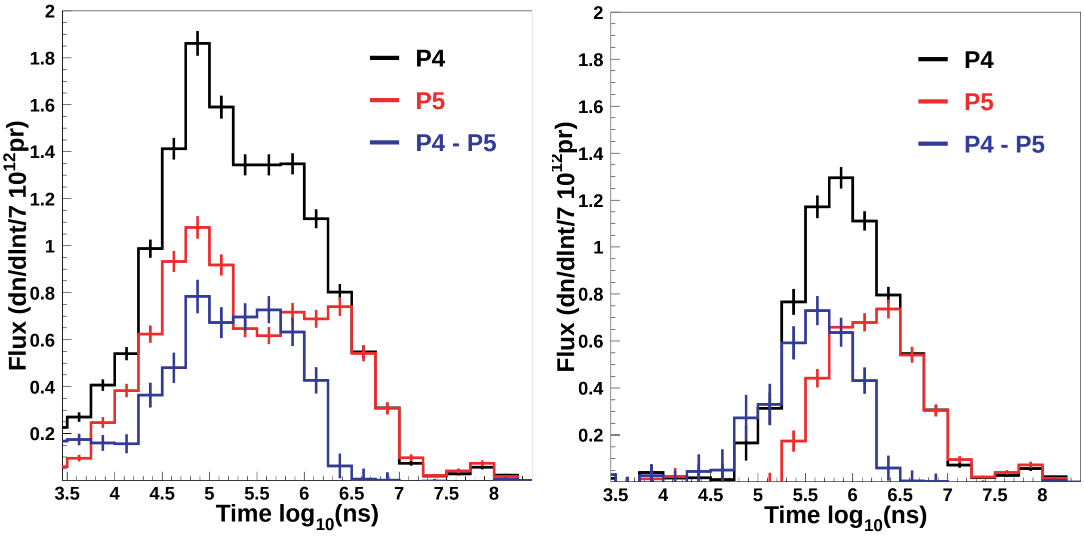

Figure 7. Left-right asymmetry measured with the ^{3}He detector in positions 4 and 5 during the reference measurement in different configurations. The black line refers to the measurement in position 4, the red line to position 5. The blue line is the difference between position 4 and 5. *Left*: measurements with small polyethylene sphere, *right*: thermal part (without correction for the efficiency), obtained from the difference between small polyethylene and small polyethylene + Cd.

3.1.3 Measurement #1: Effect of the 40 cm Concrete Wall

A 40 cm thick wall (Figure 1) made up of normal and barytic concrete blocks was placed in front of the main concrete shielding to determine whether the neutron background in the experimental area originated from fast neutrons or from muons. The data were taken in positions 4 and 5 with the ^{3}He detector inserted in a small polyethylene sphere covered and not covered with cadmium.

A reduction factor of about 3 was expected for fast neutrons, and of the order of 20-30% for muons.

Figure 8 shows the time spectra measured in position 4. The impact of the 40 cm wall is reflected in a 14% reduction of the overall neutron background in the experimental hall, measured with the small polyethylene sphere. The reduction is the same in both positions 4 and 5. Considering only thermal neutrons, the reduction is of 22% on the right side and of 11% on the left side.

These results clearly support the muon hypothesis from the Monte Carlo simulations. The reduction is slightly lower than indicated by the calculations. The poorly known composition and density of the concrete bricks of the wall, as well as the fact that the wall was built only up to the height of the collimator, may explain the difference.

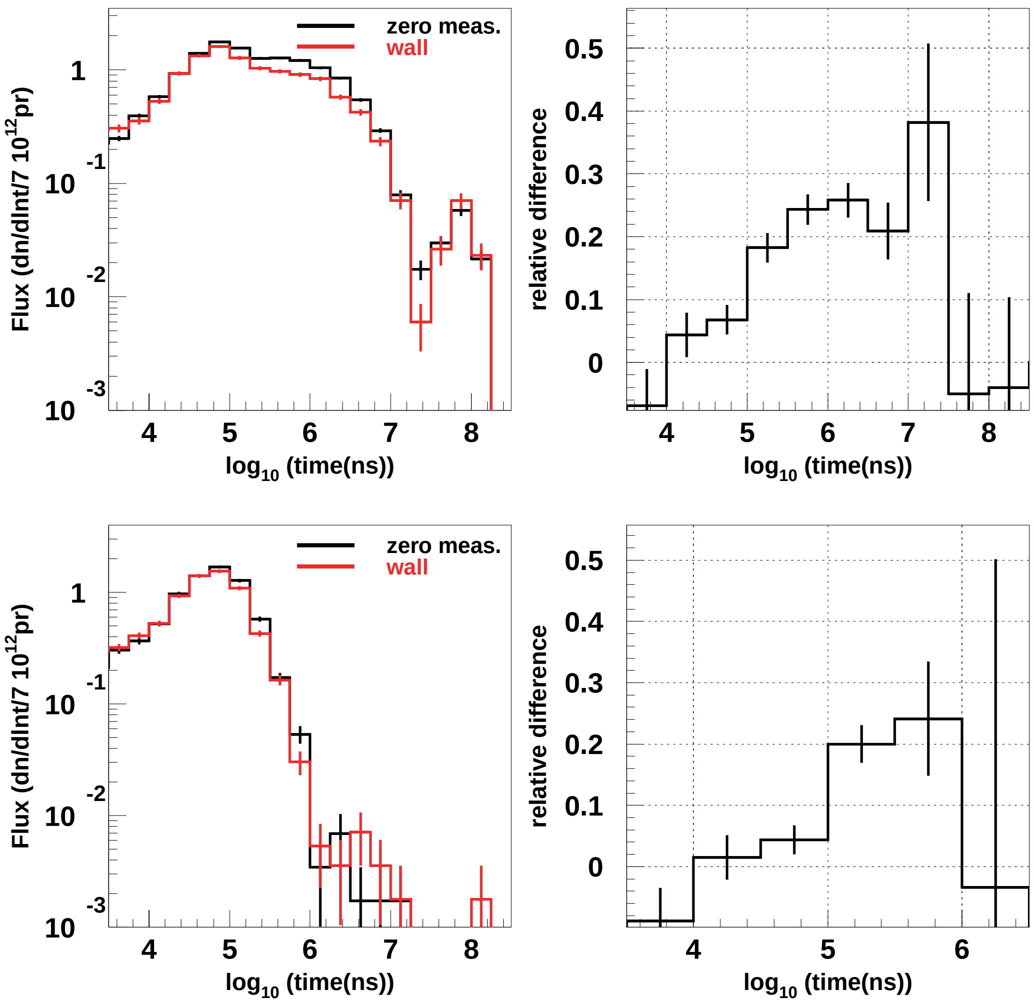

Figure 8. Effect of the 40 cm wall on the count rate measured with ^{3}He in position 4 with small polyethylene (top left) and small polyethylene + Cd (bottom left). The right-side plots represent the relative differences (difference of reference measurement and wall divided by the reference measurement) as a function of time.

3.1.4 Measurement #2: Effect of the Beam Stopper

The measurements previously described provide strong indications on the muon origin of the background, but they do not unambiguously eliminate the possibility that at least a fraction of the background could be related to the neutron beam. In order to estimate the beam-related background, measurements were performed with a beam stopper in. The beam stopper consisted of a cylindrical iron bar, 1.1 m long, inserted into the first collimator, about 47 m upstream of the experimental area.

The data were taken at position 4 with the ^{3}He detector inserted in the small polyethylene sphere with and without cadmium. The normalized time spectra are plotted in Figure 9. Compared to the measurements with the 40 cm concrete wall, the beam stopper brings a further reduction close to 8% (6% in position 5). There are no neutrons arriving at times later than 1 ms with the beam stopper in, which reveals that this component of the background is beam related, as expected.

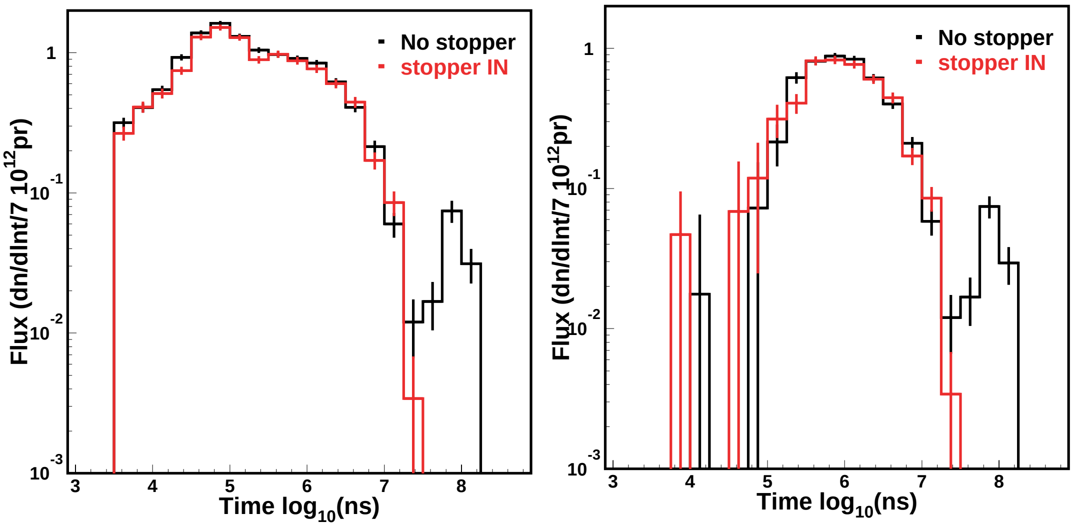

Figure 9. Effect of the iron beam stopper on the count rate measured with ^{3}He in position 4 with small polyethylene (left) and difference between small polyethylene and small polyethylene + Cd (right).

3.1.5 Effect of the Carbon Sample

An estimation of the neutron background induced by a sample placed in the beam was performed with a 6.35-mm thick carbon sample. This measurement took place with the ^{3}He counter in position 4, surrounded by the small polyethylene sphere, in measurement #0.

The count rate without any sample in the neutron beam is 8.29 ± 0.09 counts/bunch and 9.00 ± 0.09 counts/bunch when the carbon sample is inserted in the beam. The count rate is therefore increased by about 8%, mainly in the low-energy domain. Figure 10 shows the neutron flux in the two cases *(left)*; the main relative increase is for times longer than 10 ms, corresponding to thermal neutrons.

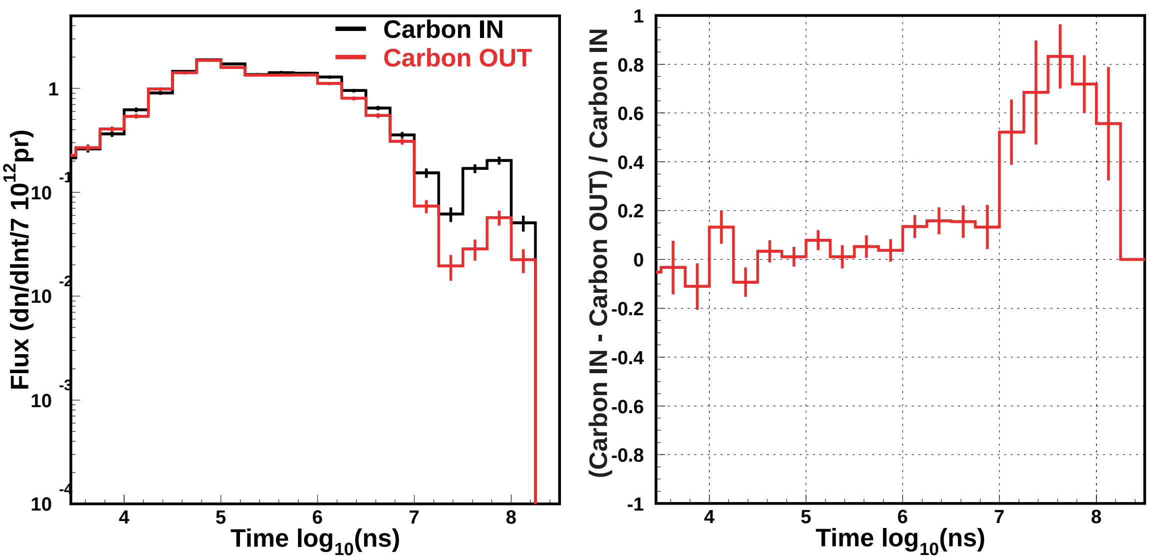

Figure 10. Increase of the neutron background from a 6.35-mm thick carbon sample in the beam.

3.2 GAMMA-RAY MEASUREMENTS

With the aim of collecting information on the origin of the γ-ray background, two C_6D_6 liquid scintillators from Bicron, provided by the CEA-Saclay team, were used. As for the ^{3}He counter, the effect on the background of different changes in the experimental conditions was investigated. These measurements were expected to complement the large body of information already collected in the May/June campaign and presented in Ref. [1].

In most of the runs, one C_6D_6 detector was kept at a fixed position, facing the sample (as in a standard measurement), while the other one was moved around the experimental area in the positions shown in Figure 3. A hardware threshold of about 85 keV and about 66 keV electron equivalent (keVee) was kept during the measurements on the fixed and movable detector, respectively. The detector output was sent through a fast timing amplifier and then split in two: one branch to a constant fraction discriminator was used to stop a multi-hit TDC; the second branch was amplified through a spectroscopy amplifier, then recorded with a 40 MHz flash ADC.

The C_6D_6 measurements were complemented with measurements of activation γ rays using one HPGe detector from CEA-Saclay. These activation measurements are presented next.

3.2.1 Activation Measurements

For high-resolution γ spectrometry we used one HPGe detector (Canberra model GR25195-7935.7S) with the following characteristics: coaxial one open end, diameter 52.5 mm, length 56 mm, relative efficiency 25%, energy resolution 1.95 keV FWHM at 1.33 MeV. For energy and efficiency calibration ^{60}Co and ^{152}Eu γ-ray sources were used. Standard NIM electronics was used for the measurement.

The detector was placed in the experimental room, 30 cm from the sample exchanger (at the right looking from the target), 50 cm below the beam line. Only measurements without beam were taken.

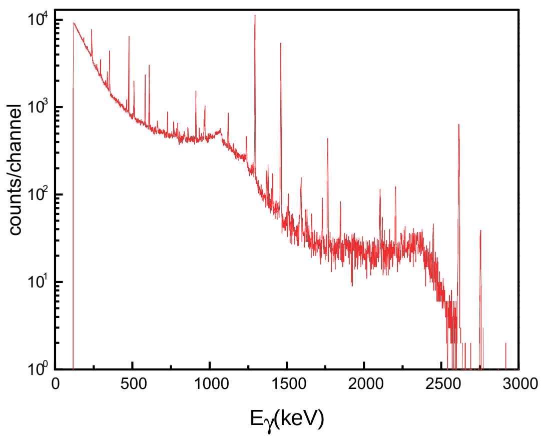

Figure 11. Gamma spectrum measured with the HPGe detector 3.5 hours after the beam stop (left), and background-subtracted spectrum showing the short-lived component (right).

The γ spectrum from run 921, taken 3.5 hours after the beam stop, is shown in Figure 11 (left plot). The γ-ray peaks present are of ^{232}Th decay products (239, 510.6, 583, 727, 860, 969, 2614 keV), U-Ra radioactive family (609, 768, 1120, 1764, 2248 keV), ^{40}K (1461 keV), activation products ^{41}Ar (1293 keV), ^{24}Na (1368, 2754 keV), spallation product ^{7}Be (477.6 keV), positron annihilation (511 keV).

The presence of short-lived activation products is evident after subtracting the γ background from the measured spectra, as shown in the right-side plot of Figure 11. The 511 keV annihilation peak and the 1293 keV ^{41}Ar γ line are clearly observed. Therefore they should be the main sources of additional γ background which is not directly beam related.

The time dependence of the activity could not be obtained directly from the peak areas because of the long dead time of the detector. Therefore we used the potassium 1461 keV line as a reference. The intensities of the annihilation and ^{41}Ar γ lines as a function of time after the beam stop are shown in Figure 12. For both lines a rough exponential decay is observed. Concerning the 511 keV line, many reactions can lead to this γ ray. In the case of ^{41}Ar there are fluctuations from the exponential. There is even an increase of argon activity 21 hours after the beam stop. Clearly, the variation of air circulation from the tunnel to the experimental hall strongly affects the intensity of this line.

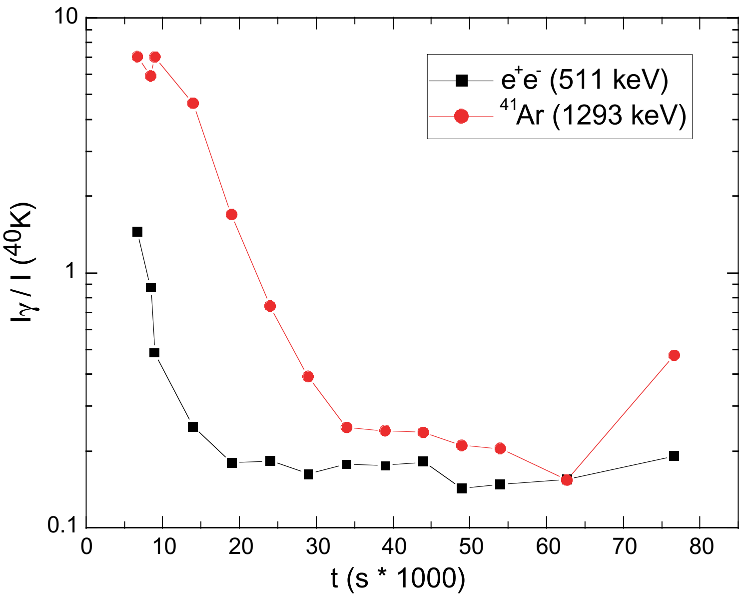

Figure 12. Intensity of the annihilation and ^{41}Ar lines (normalized to the ^{40}K line) as a function of time, measured in the experimental station, without beam, starting right after the end of a long physics run.

The presence of γ rays from activation was also evident from C_6D_6 measurements.

Figure 13 shows a background spectrum (black histogram), measured with a C_6D_6 in the fixed position with no sample in place, normalized to the reference n_TOF bunch of 7×10^{12} protons. On the horizontal axis the recording time has been converted into neutron energy in order to illustrate how the various energy zones are affected. This neutron energy scale is used for all C_6D_6 plots. In Appendix A a figure gives the correspondence between the time and the neutron energy for a flight path of 186 m.

When compared above 1 eV, the measured background is similar, as expected, to the one measured in May/June (green histogram). A small difference in the absolute level is observed; this is probably due to the slightly higher detector threshold in the new measurements and also to the different amount of material present in the experimental area. The trend at large time-of-flights (up to 100 ms), evidenced the presence of a further background component, which had not been previously investigated. In agreement with the HPGe results, this component was attributed to air activation (^{41}Ar), most probably produced in the primary zone and flowing to the experimental area.

The data shown in the figure were taken after a few days of running with high proton intensity, so that a large activation had already built up. In the present conditions, the background due to activation may contribute significantly up to few hundreds eVs. Therefore, in order to perform a meaningful comparison between different runs down to the eV region, an effort was made to estimate and subtract the activation component, whose level may significantly differ from run to run depending on several factors (beam intensity, build up time, differential air pressure, etc.). The level of the activation-related background in the different measurements is estimated by means of an exponential fit performed in the region between 25 meV and 1 eV. The corresponding function (blue curve in Figure 13) is then subtracted from the original spectrum at all energies to obtain an activation-free spectrum (red histogram).

The assumption that the observed exponential behaviour associated with activation holds valid over a large energy range was checked by subtracting the normalised spectra measured at different periods with the same detector and experimental conditions. As expected, a pure exponential trend is observed over the whole range (insert of Figure 13), with the decay constant of 1.15 corresponding to a flat time-of-flight distribution.

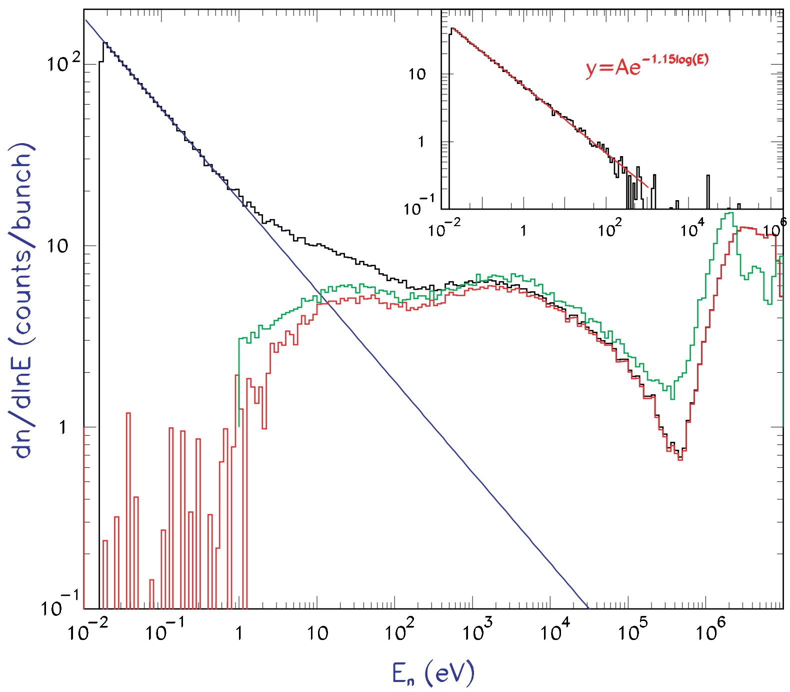

Figure 13. Gamma-background spectrum, measured with a C_6D_6 detector at the sample position (black curve). The activation-free background spectrum (red histogram) is compared with the background measured in the May/June campaign with the same detector in the same position, with the standard n_TOF DAQ (green histogram). In the insert, the subtraction of background spectra taken at different times in the same running conditions shows an exponential trend in logarithmic scale, as expected from a constant activation background.

Some tests were performed to investigate possible remedies to the activation-related background. Figure 14 shows the level of activation as a function of the run number. Starting from run 886, a rough sealing of the experimental area from the secondary area was attempted, which resulted in a decrease of the activation level, as evident in the figure (on the average, the activation level is reduced by a factor of 3). Since after the installation of the 3.2 m iron wall the contribution of the activation to the overall background becomes significant, even in the keV region, a more accurate sealing of the experimental area from the secondary zone was undertaken. After the intervention, a further reduction of the activation level was achieved (green symbols). As a countercheck, the last run, just before the PS shutdown, was recorded with the door to the secondary area open.

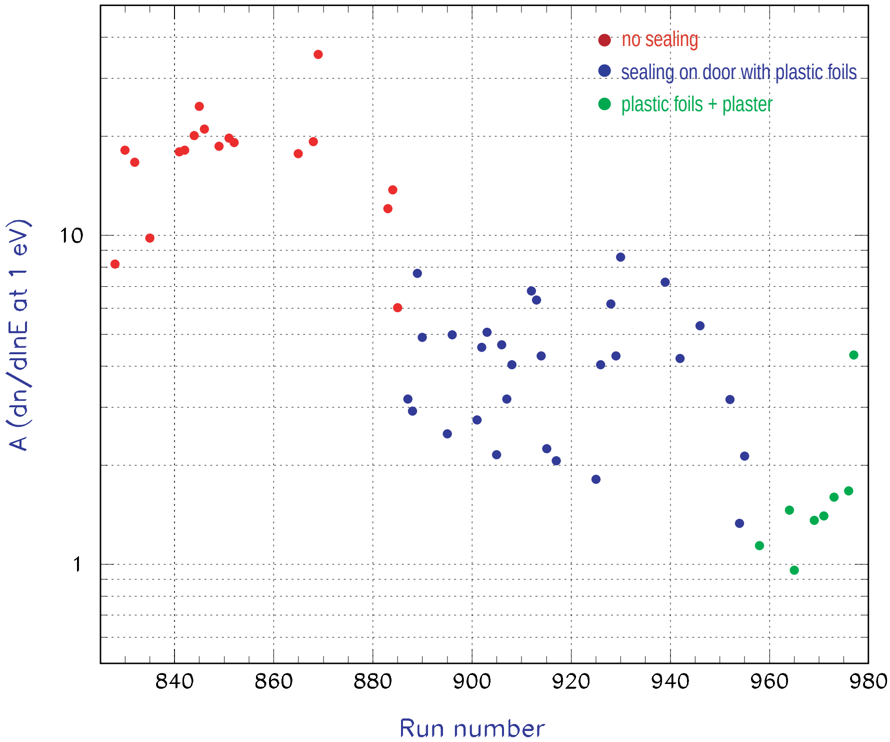

Figure 14. The activation-related background in various configurations as a function of the run number. See explanation in the text.

3.2.2 Reference Measurements: Left-Right Asymmetry and Effect of the Magnet

Figure 15 shows the background measured with the C_6D_6 at different positions inside the experimental area. In agreement with the results of the ^{3}He counter, the measurements with C_6D_6 do not indicate a strong asymmetry of the "slow" background component. The largest background is observed in position 4 (close to the wall between experimental and secondary area, on the right when facing the escape lane), but even in this case the difference with position 5 is less than a factor of two. A measurement performed with the C_6D_6 very close to the right-side wall (position 0) shows only a 20% increase.

A potential influence of the magnetic field and its polarity was investigated by switching the magnet on and off and reversing polarity. With the magnet off, a systematically higher background was observed, with a difference of the order of a few percent. Although small, this effect could become significant when the largest background component is suppressed.

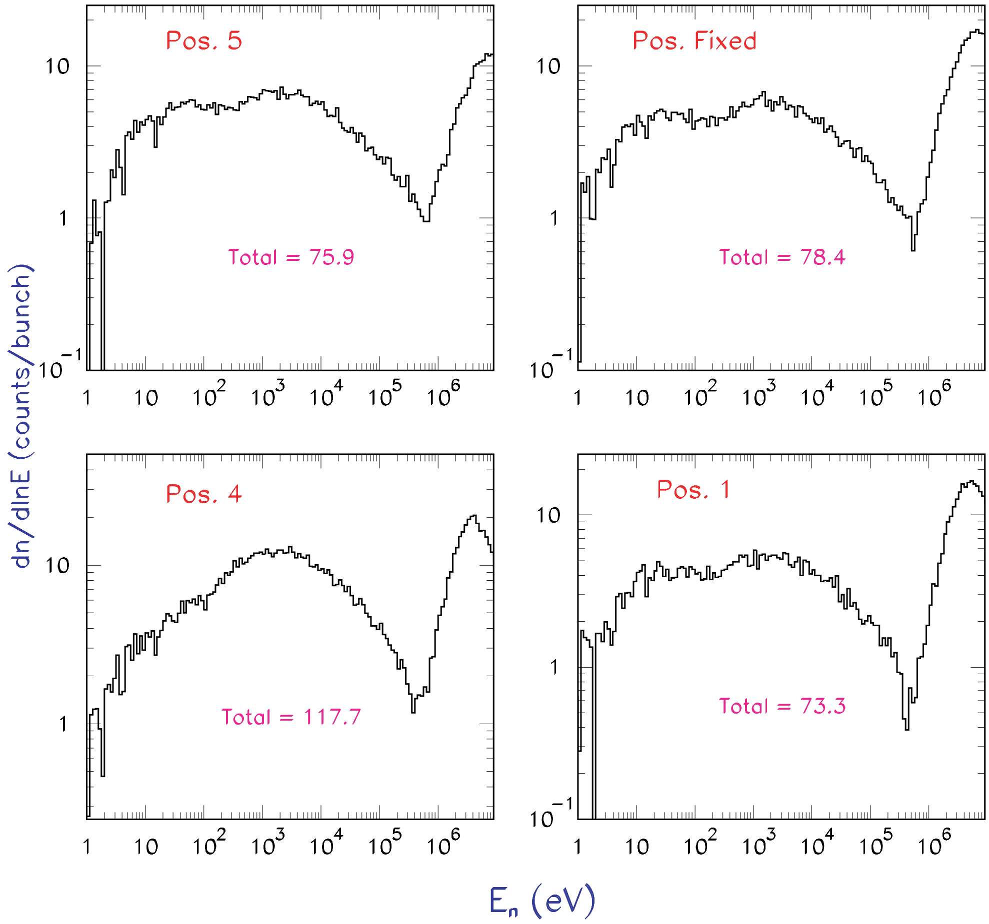

Figure 15. The γ background (after subtraction of the activation) measured at different positions inside the experimental area.

3.2.3 Measurement #1: Effect of the 40 cm Concrete Wall

The effect on the background produced by the addition of a 40 cm concrete wall on the right side of the experimental area is shown in Figure 16. As roughly expected from the muon-related background hypothesis, and in agreement with the results of the ^{3}He counter, a difference of the order of 15% is observed on both sides of the beam (at the level of the sample). The ratio between the spectra taken before and after the addition of the wall (bottom panels of Figure 16) indicates that the effect is uniform over the whole energy region, consistent with the attenuation of the primary source of neutrons.

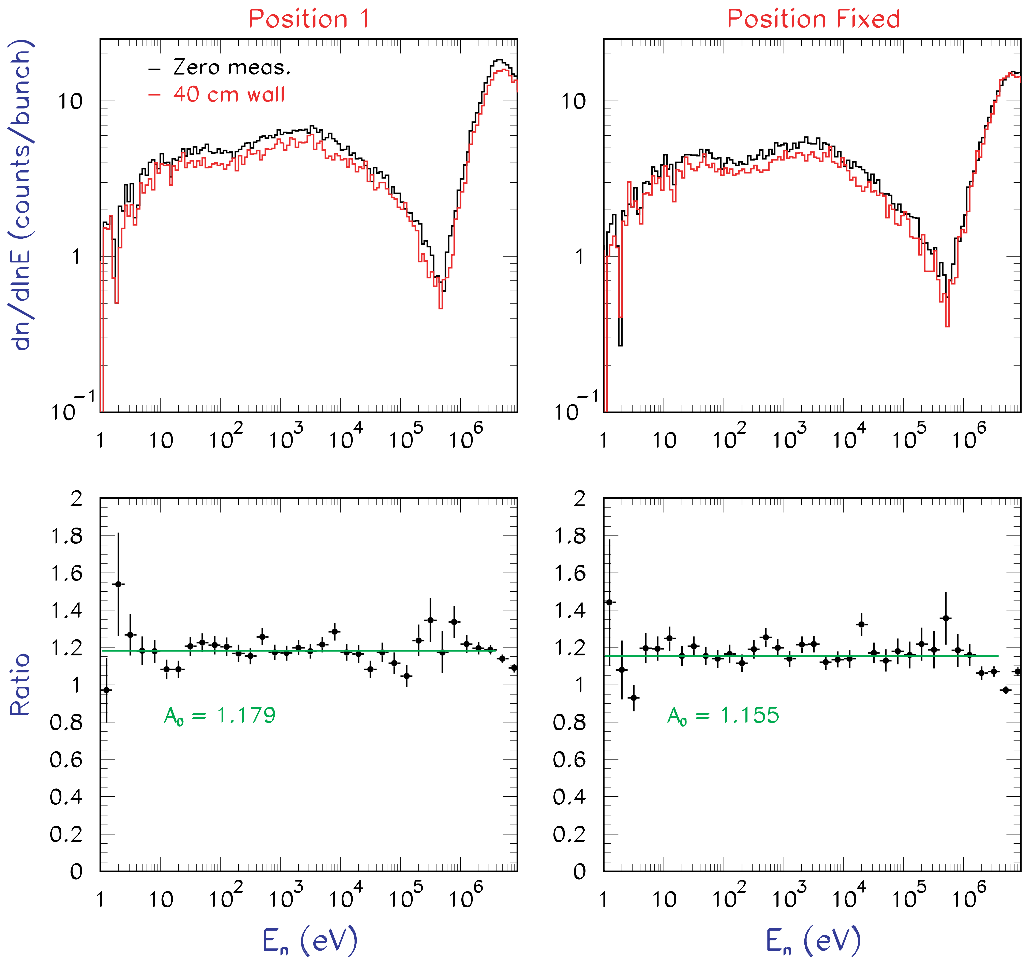

Figure 16. Effect of the addition of a 40 cm wall at the interface between secondary and experimental area. The ratio between the spectra is shown in the bottom panels. A linear fit of the ratio indicates an average effect between 15 and 20%, depending on the position inside the experimental area.

3.2.4 Effect of the Carbon Sample

The effect of the sample on the background was further investigated before proceeding with modifications of the facility. To complement the results already presented in the Status Report, the effect on the γ background of neutrons scattered from the carbon sample was measured at different positions inside the experimental area (Figure 17). Consistent with Figure 5-11 of Ref. [1], a significant increase of the background is observed close to the sample. In the other positions, however, the effect is much smaller. Solid angle considerations point out to the source of the bump being close to the sample, or being the sample itself. The "residual" increase of the background due to the carbon sample, relative to the no-sample case, is of the order of 5 to 10%, uniformly distributed over the energy range and approximately independent of the position inside the experimental area.

Combined with the results of the ^{3}He counter, these measurements indicate that neutrons scattered from the sample may contribute to a non-negligible increase of the diffused γ-ray background. This background is presumably generated by the same process which the muon-produced neutrons undergo, i.e. capture in the walls of the experimental area or in other material present therein. In addition to this, another source of background should be considered close to the sample, probably related to in-beam γ rays. As shown in Ref. [1], however, such a source is characterised by a noticeably soft spectrum, so that the application of the pulse weighting technique may considerably reduce this component.

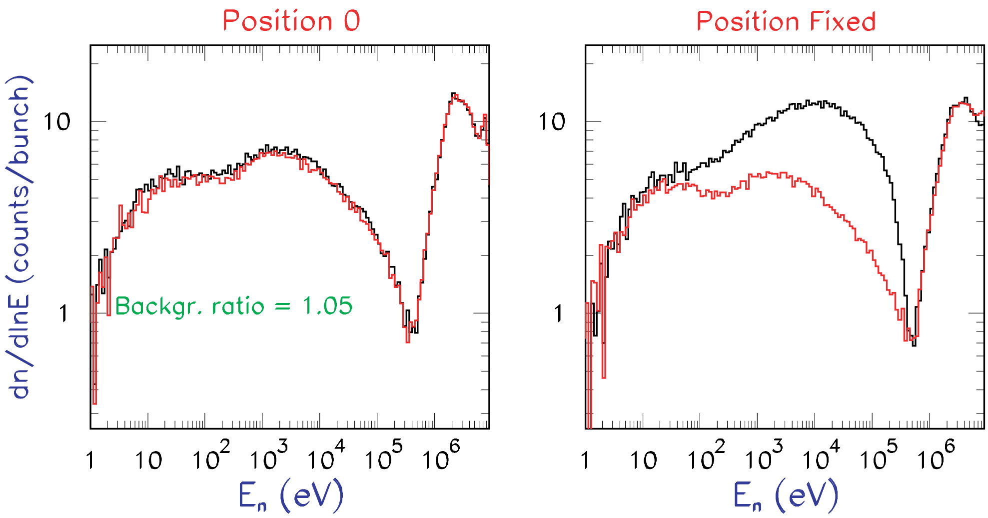

Figure 17. Comparison between background spectra relative to no-sample (red histogram) and C-sample (black histogram), for two different positions inside the experimental area. At large distances from the sample (position 0) the 6.35-mm carbon results in a uniform increase of the background of the order of 5%. Close to the sample, an additional soft γ-ray source is observed.

An analysis of the spectra of the C_6D_6 detectors using FADC data was carried out. The time-of-flight spectra obtained from the FADC without any supplementary threshold other than the electronic threshold of ~85 keV is shown in Figure 18 for the detector in the fixed position. In order to investigate the nature of the detected γ-ray spectrum, we applied different software thresholds of 200 keV and 500 keV on the FADC data. The decrease of the spectrum with increasing threshold is clearly visible for the detector close to the sample position with the carbon sample in the beam, while without the carbon sample the decrease is only visible at much higher thresholds. This represent a further proof that the strong background enhancement observed close to the sample is characterized by a soft γ-ray spectrum.

A check of the influence of a weighting function, which emphasizes more the events with high γ-ray energy than those with low amplitudes, was performed. Applying to each event a weight proportional to its amplitude, which is the effect of a linear weighting function, the spectra shown in the bottom-right plot of Figure 18 is obtained; a cut on the amplitude of 85 keV was applied. As expected, a decrease of the difference is well noticeable, although the effect of the sample is still visible. Further analysis with a more realistic weighting function should help to quantify this effect more precisely.

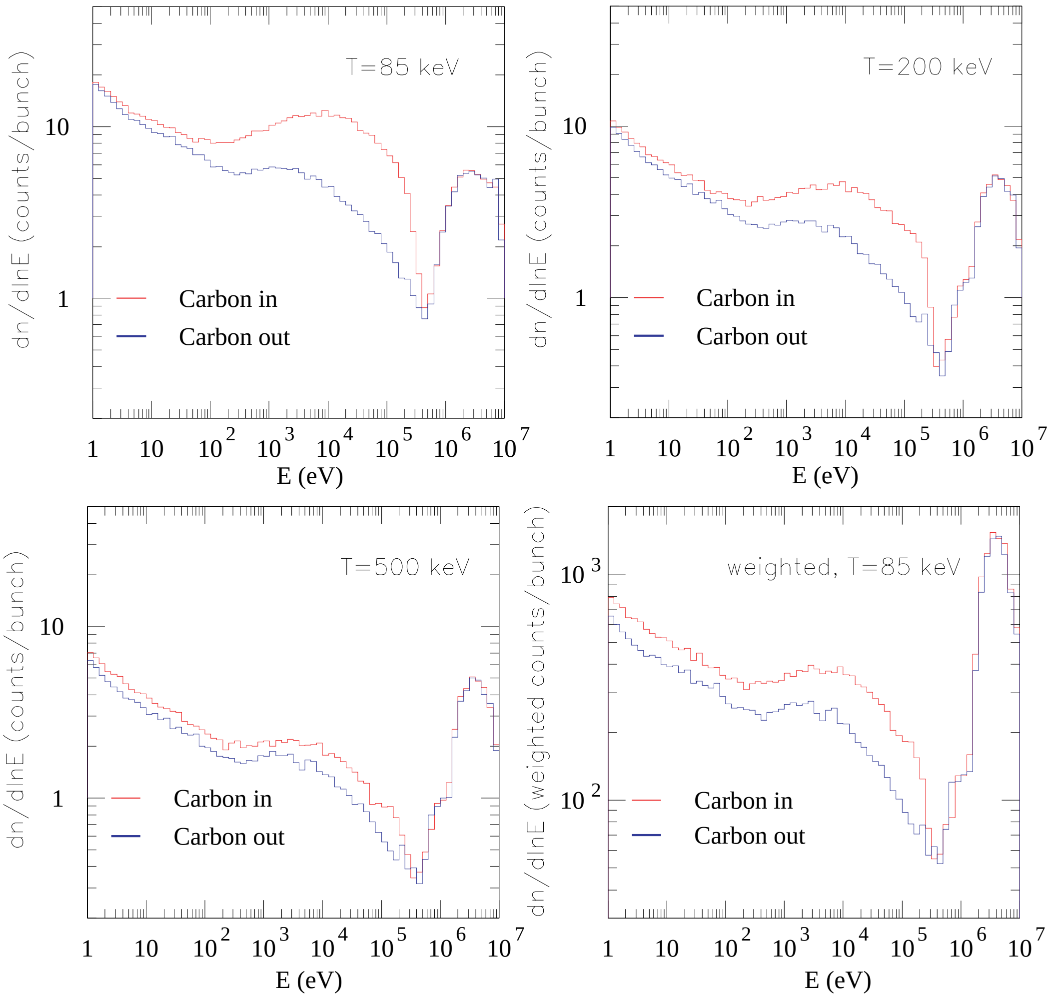

Figure 18. Time spectra of the C_6D_6 detector in fixed position, with and without the carbon sample, obtained from the analysis of the FADC data. The electronic threshold of 85 keV and software thresholds of 200 and 500 keV were applied. The decrease of the bump due to the presence of the carbon sample is evident. The bottom-right panel shows the effect of a linear weighting function. The influence of the soft γ rays is attenuated but not completely wiped out.

3.2.5 Measurement #2: Effect of the Beam Stopper

An analysis of the C_6D_6 data taken with the beam stopper inserted in the first collimator was also performed in order to estimate the beam-related background.

Figure 19 shows the ratio between the background spectra measured immediately before and after the insertion of the beam stopper, in two different positions inside the experimental area (one close to the sample and one facing the entrance wall of the area). The difference is slightly above 7% for the detector close to the sample, uniform over the whole energy range except at higher energy. For position 4, the ratio is higher (12%). However, it cannot be excluded that the difference was due to a slightly different position and/or orientation of the detector between the two runs.

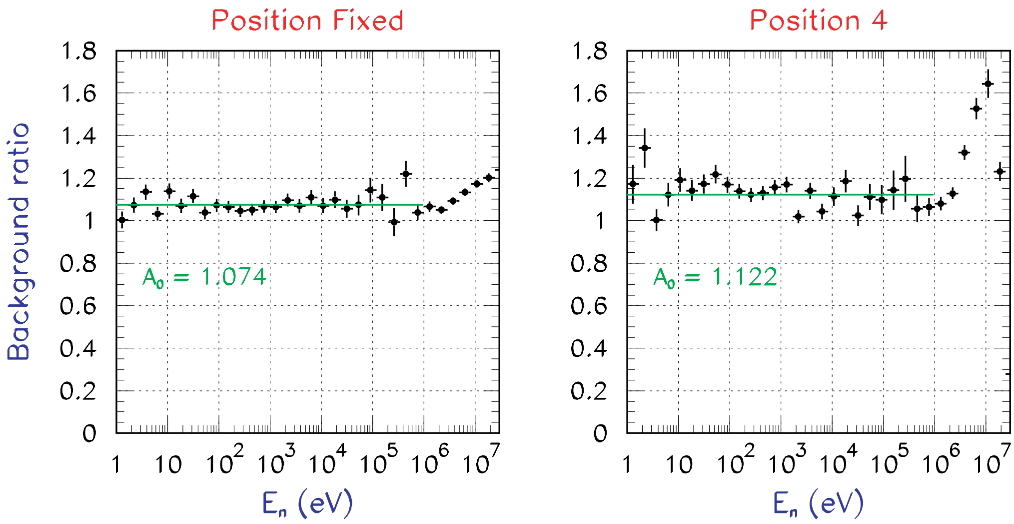

Figure 19. The ratio of background spectra collected before and after the insertion of the beam stopper at the level of the first collimator indicates that a fraction between 5 and 10% could be attributed to beam-related effects.

3.3 CONCLUSIONS FROM THE FIRST PHASE OF MEASUREMENTS

The cause and the features of the background existing in the n_TOF measuring station were carefully studied [2] and measured as detailed above, using mainly ^3He and C_6D_6 detectors. A good agreement was found between the data collected with both counters.

During the reference measurement, higher count rates were observed on the right side of the measuring station compared to the left side, looking from the target. This asymmetry was found to be greater close to the wall separating the second collimator to the room, than in the middle of the room. Actually, the asymmetry in the count rates as measured with the ^3He in these respective locations was of 35% (up to 63% for fast neutrons) and of 8%.

After installing the 40 cm concrete wall, the count rate was only reduced by 14%, on the overall time spectrum. This definitively confirmed the neutron production hypothesis by the muonic capture process in the surrounding walls and materials as suggested by the simulations.

The next step consisted of stopping the beam with a 1 m long iron bar installed in the first collimator. The total count rates were further decreased by 7%. Events arriving later than 1 ms were no more observed, proving the beam-related nature of this background component.

Finally, with the presence of a 6.35-mm thick carbon sample placed in the neutron beam, the count rates increased from 5 to 10% depending on the distance of the detector from the sample.

Gamma measurements were taken without beam in the experimental hall with a high-purity germanium detector. Two main γ rays resulting from activation, namely the 511 keV annihilation peak and the ^{41}Ar line of 1293 keV (air activation) were observed. These results are in agreement with measurements done in July 2001 (Ref. [4]).

The area was completely sealed to reduce the air flow from the target zone. As a result the γ background due to activation was decreased by approximately one order of magnitude.

The measurements with the C_6D_6 and ^3He in different positions and the effect of different changes in the experimental conditions, in particular the 40 cm wall and the beam stopper, combined with the simulations, gave sufficient indication of the negative muon origin of the slow background component. The simulations also indicated how to effectively reduce the background [2]. It was therefore decided to proceed with the installation of a 3.2 m thick iron shielding just after the magnet, aimed at significantly reducing the muon flux in the experimental area.

4. MEASUREMENTS AFTER INSTALLING THE IRON SHIELDING

After installing the 3.2 m iron wall, the background measurements were repeated with the detectors in the same conditions as in the first phase. Since a lower counting rate was expected after the shielding installation, measurements were performed with the ^{3}He detector in positions 4 and 5 only, and with the C_6D_6 counters in positions 1 and fixed.

4.1 NEUTRON MEASUREMENTS

Three different measurements were performed after the installation of the iron shielding, and similarly to the previous ones, namely: with the beam stopper (*measurements #3*), without the beam stopper (*measurements #4*) and without the beam stopper and with the 40 cm thick concrete wall (*measurements #5*). The results are shown in Table 2. For measurements #3 and #5 the time spectra measured with the ^{3}He with the small polyethylene sphere are shown in Figure 20 (blue and red line, respectively). They are compared with the spectra from measurements #0 and #2 (black and green line, respectively). Measurement #4 gives spectra very close to measurement #5 and therefore is not shown.

Table 2. Counts per 7×10^{12} protons with the ^{3}He detector in different positions and configurations during the measurements #3, #4 and #5, taken after the installation of the 3 m iron wall. The statistical uncertainties on the detector counts are indicated.

Position #	Small poly	Small poly + Cd
MEASUREMENT #3: IRON WALL+ BEAM STOPPER		
4	0.196 ± 0.013	0.120 ± 0.005
5	0.113 ± 0.008	0.070 ± 0.004
MEASUREMENT #4: IRON WALL, BEAM STOPPER OUT		
4	0.476 ± 0.015	
5	0.552 ± 0.032	
MEASUREMENT #5: IRON WALL+40 cm WALL, BEAM STOPPER OUT		
4	0.446 ± 0.015	
5	0.546 ± 0.019	

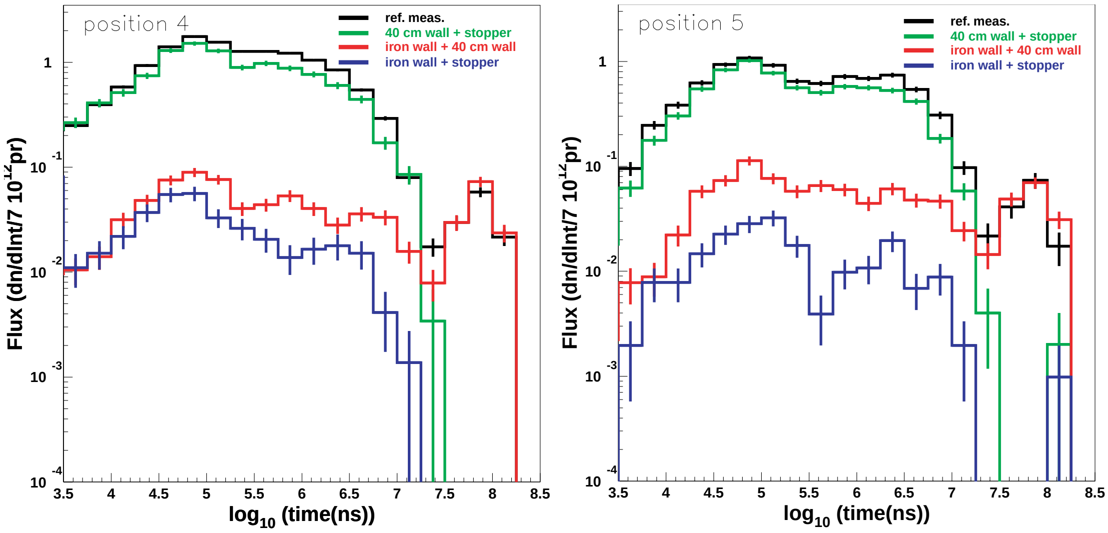

Figure 20. Background reduction measured with the ^{3}He detector with small polyethylene sphere in positions 4 and 5. Black line: measurement #0; green line: measurement #2; red line: measurement #5; blue line: measurement #3.

The background reduction after the installation of the iron wall is estimated by comparing measurements #0 and #4. The reduction factor is of about 17 on the right side, and about 9 on the left side.

A stronger reduction of the neutron background is observed when the beam stopper is inserted: a factor of about 32 on the right side and about 37 on the left side is obtained when comparing measurements #2 and #3.

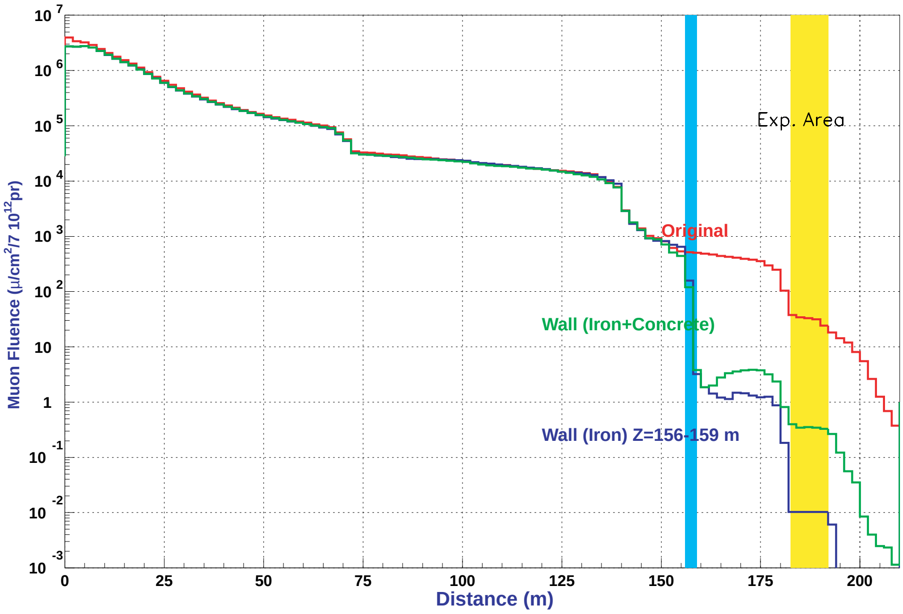

Figure 21. Simulated average muon flux as a function of the distance from the lead target for a standard pulse of 7×10^{12} protons. Red curve: configuration without iron shielding. Green curve: iron shielding with concrete base. Blue curve: iron shielding. In the simulations the shielding closes the whole section of the tunnel.

In addition to the simulations presented in Ref. [2], further calculations were performed to estimate the effect of a concrete base. In Figure 21 the simulation of the average muon fluence in the n_TOF tunnel is shown. The fluence is calculated in a rectangular area of 2×3 m^2 around the beam tube. Results are presented without any shielding, with a pure iron shielding and with an iron shielding with a concrete base 1 m high. The latter configuration is the closest to the experimental one. However, contrary to the real case, in the simulations the wall closes completely the section of the tunnel, without any openings. From these simulations the average fluence values in the experimental area in the three configurations are 34 μ/cm^2/7×10^{12} protons, 0.01 μ/cm^2/7×10^{12} protons and 0.35 μ/cm^2/7×10^{12} protons, respectively. Thus, background reduction of a factor 100 is expected with an iron/concrete shielding. The discrepancy with the observed reduction is probably due to the holes in the shielding and/or to the chicane.

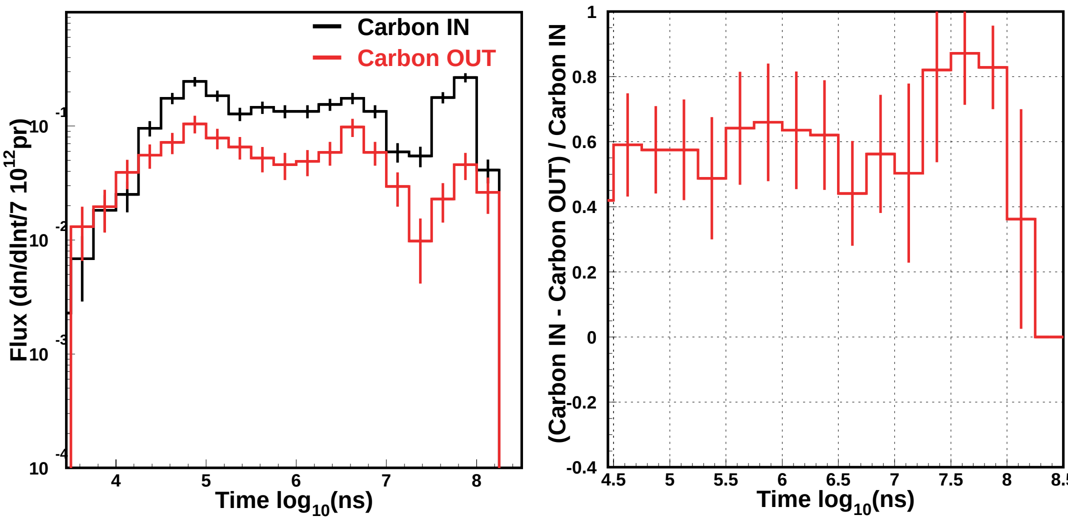

Figure 22. The sample-related background after the installation of the iron shielding. *Left*: time spectrum of the ^{3}He detector with small polyethylene sphere with and without C sample. *Right*: relative difference.

By comparing the background attenuation with and without beam stopper, it is obvious that after installing the shielding the beam-related component of the background acquires a much higher relative importance in the overall balance: the fraction of the background which is beam related is now about 60% on the right side, and about 80% on the left side (see Table 2).

After removing the beam stopper, the previously observed asymmetry between positions 4 and 5 is reversed. This may be due to streaming of neutrons in the chicane at the left of the measuring station.

Additional series of measurements were done with carbon, gold and iron samples in the beam. The time spectra for the thick (6.35 mm) carbon sample are presented in Figure 22 for the detector with the small polyethylene sphere placed in position 5. The increase of the ambient background due to the presence of this sample is of a factor 2.5. The background brought by the neutron scattering process observed with the three different samples is given in Table 3.

Table 3. Total count rates (counts/7×10^{12} p) in presence of different samples in the neutron beam. The increase factor *f* is indicated.

Sample and thickness	Position	Sample OUT	Sample IN	*f*
Au (0.1 mm)	5	0.546 ± 0.019	0.595 ± 0.007	1.1
Fe (1.5 mm)	4	0.446 ± 0.015	0.819 ± 0.049	1.8
C (6.35 mm)	5	0.546 ± 0.019	1.351 ± 0.14	2.5

The effect of the magnet with the facility in the present conditions was studied. A measurement was taken with the ^{3}He detector in position 5 (Figure 23). The count rate with the magnet OFF is 1.09 ± 0.05 counts/7×10^{12} p, with the magnet ON is 0.54 ± 0.02 counts/7×10^{12} p. Therefore, the effect is of about a factor 2, indicating that a high background is generated when charged particles pass through the tube.

A similar test had been done before the iron shielding installation, giving a negligible effect.

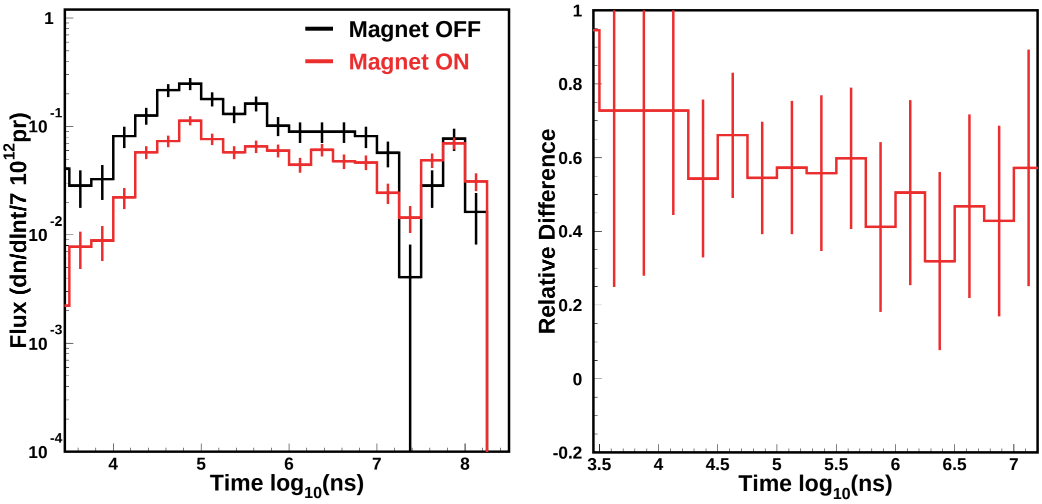

Figure 23. ^{3}He time spectra measured in position 5 with magnet on/off (left) and the relative difference (right).

4.2 GAMMA-RAY MEASUREMENTS

4.2.1 Gamma Background Reduction

After the installation of the iron wall in the secondary area, measurements with the C_6D_6 detectors were repeated, in order to determine the new background conditions.

An extra C_6D_6 scintillator from CEA/Saclay was used with the n_TOF data acquisition system [1]. A typical FADC signal from this detector recorded immediately after the γ-flash is shown in Fig. 24. The amount of background has been significantly reduced, compared to Fig. 5-7 of Ref. [1] representing the same signal recorded during the May campaign of measurements.

As already mentioned, the main feature of the fast background components (arriving within 20 μs) was the strong dependence on the position inside the experimental area with the right-hand side being significantly more enhanced. A left-right asymmetry is still visible in the present data for the fast domain.

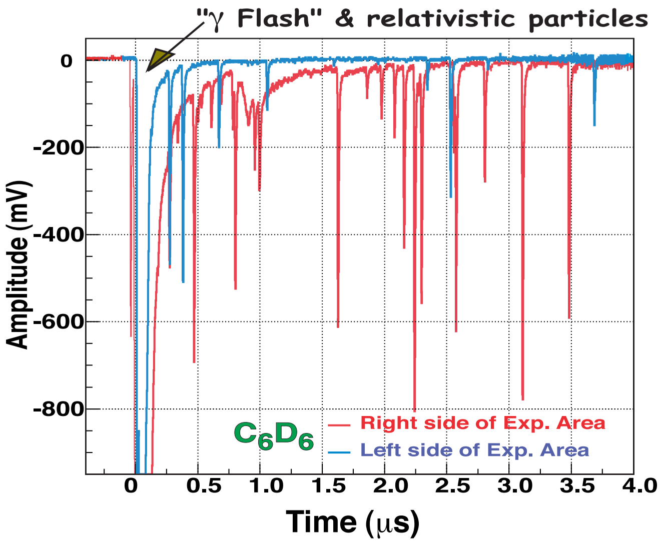

Figure 24. A typical history of the C_6D_6 FADC signals immediately after the γ-flash under the present shielding conditions, in position 1 (right side) and fixed (left side).

The sample related background in the present configuration has been studied by inserting a 6.35-mm thick carbon sample in the beam. This measurement permitted also to observe the slow component (due to activation) by looking at longer times. The time-of-flight spectrum of C_6D_6 events measured in the fixed position, with and without any carbon sample, is shown in Fig. 25a; the same events are represented on a neutron energy scale in Fig. 25b.

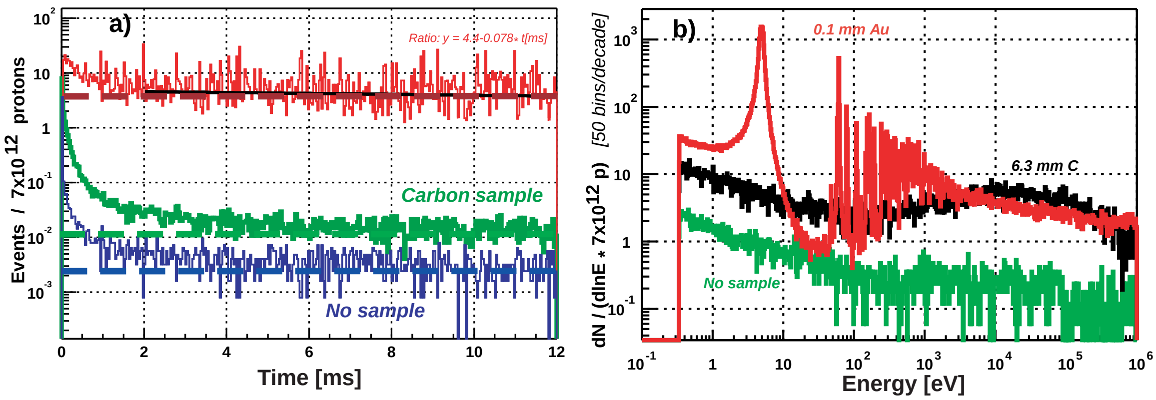

Figure 25. a) Time-of-flight spectrum of C_6D_6 events measured with and without carbon sample in the beam. b) Same spectrum plotted versus neutron energy. The spectrum with a 0.1 mm gold sample is also shown for comparison.

The time-of-flight spectrum shows significant difference with the corresponding data collected in May 2001 (see Fig. 3-16 in Ref. [1]). The number of events at later times (longer than ~1 ms) is constant as expected from the radioactive decay of ^{41}Ar.

The difference in shape between the spectra taken with and without sample in the beam appears only at times shorter than 1 ms, showing up as a bump in the energy spectrum above 100 eV (Fig. 25b). The ^{41}Ar radioactive decay in this figure is reflected as an exponential shape in the neutron energy scale (see also Fig. 13).

An overall picture of the different components of the current background, measured in the middle of the experimental area (position 1, 75 cm from the sample) with the C_6D_6 used during the first phase, is shown in Figure 26.

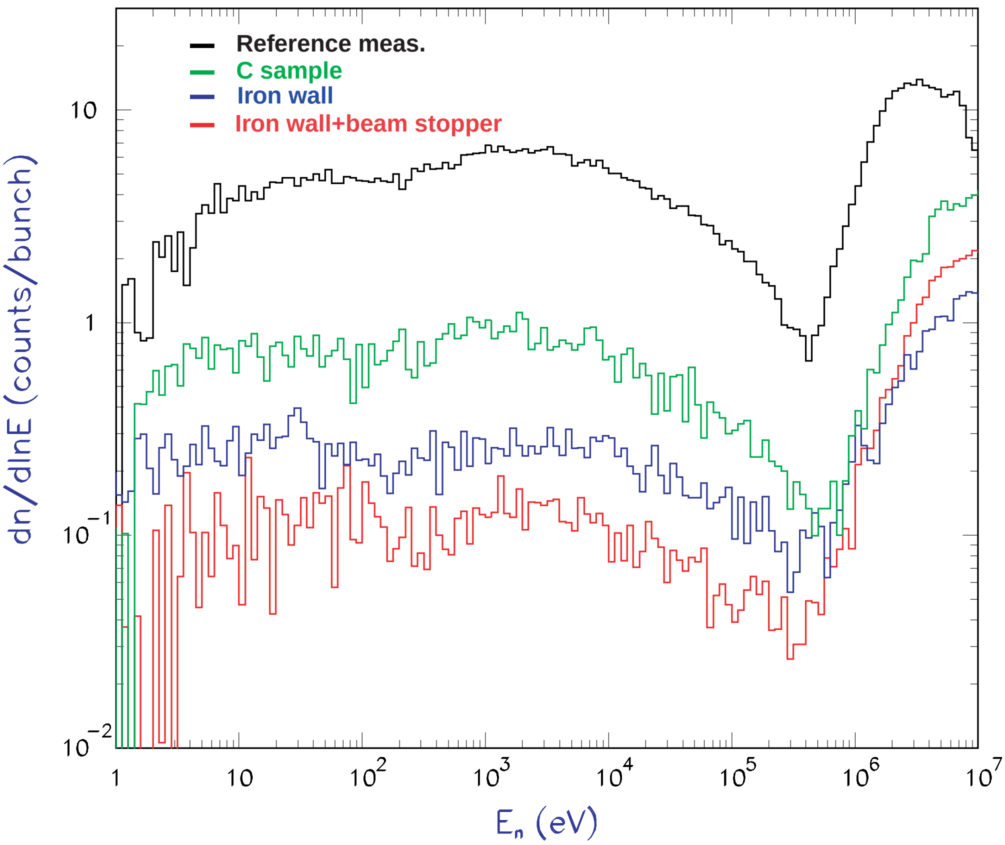

Figure 26. Comparison of the background level in different conditions, measured with the C_6D_6 in position 1. The black curve corresponds to the reference measurement. The red histogram represents the residual contribution of the muon background, after the installation of the 3.2 m iron wall, and with the beam stopper inserted in the first collimator. The beam-related component, estimated from the blue histogram, represents in the present conditions 2/3 of the overall background observed without samples. Finally, for a 6.35-mm thick carbon sample, the sample-related component accounts for about 50% of the observed background.

The red histogram represents the background with the iron wall in place, and with the beam stopper in. Relative to the original background level, a reduction of more than a factor of 40 is observed up to 1 MeV.

Considering the high energy part, events are due to muons; indeed an exponential fit of the decaying section indicated a value of 2.2 μs for the constant decay parameter corresponding to the muon half-life.

The blue histogram represents the results of the measurements done after removing the beam stopper. As already found with the ^{3}He, the beam-related background now becomes dominant. Indeed, the background level observed without the beam stopper is now approximately 2.5 times higher than with the beam stopper in. The origin of the local background was not further investigated, but likely it is associated with the reduction at the level of the second collimator, backscattering from the neutron escape lane or scattering from other elements along the beam line in the experimental area. Nevertheless, the current background without sample is approximately 15 to 20 times smaller, in the low-energy region, relative to the one observed in the May/June campaign.

As shown in paragraph 3.2.4, measurements with the carbon sample result in a further increase of the background, produced by neutrons scattered from the sample and captured in the wall of the experimental area or other material therein. While such a contribution was originally small relative to the muon-induced background, after the large reduction of the muon part with the iron wall, a much bigger effect of the sample has to be expected. The green histogram in Figure 26 shows the background observed with a thick carbon sample. The sample-related background now results in an increase of the background level by approximately a factor of 2 (with the detector in position 1).

Finally, a much larger effect is now related to the sweeping magnet, since the background increases by a factor of 2 with the magnet off (Fig. 27), in agreement with the ^{3}He measurements.

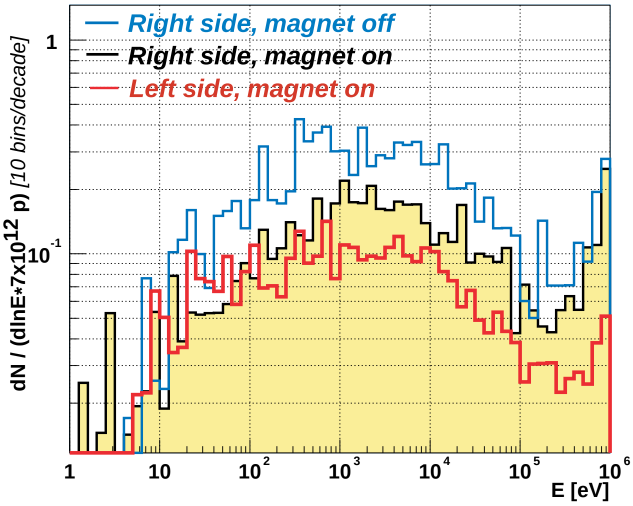

Figure 27. Spectrum measured with the C_6D_6 on the right side with magnet on and off. The spectrum obtained on the left side with magnet on is also shown.

4.2.2 Measurements of Au and Fe Resonances

The effect of the present background on the measurements of the capture cross sections was estimated by means of a 0.1-mm thick Au sample and a 1.5-mm thick Fe sample. Figure 28 shows the comparison of the count rate measured in the May/June campaign with the new situation. Although this comparison can only be taken as indicative, considering that the spectra were taken in different experimental conditions (detector threshold, material in the experimental area, etc.), a significantly higher peak-to-valley ratio is now observed. The improvement in the level of background can be also appreciated by some small resonances, which are now much more clearly identified (as, for example, the one at ~50 eV in the case of gold, and the ones indicated by arrows in the case of iron). The present background is affecting the capture measurements mainly for energies above about 100 eV, when compared to the simulations.

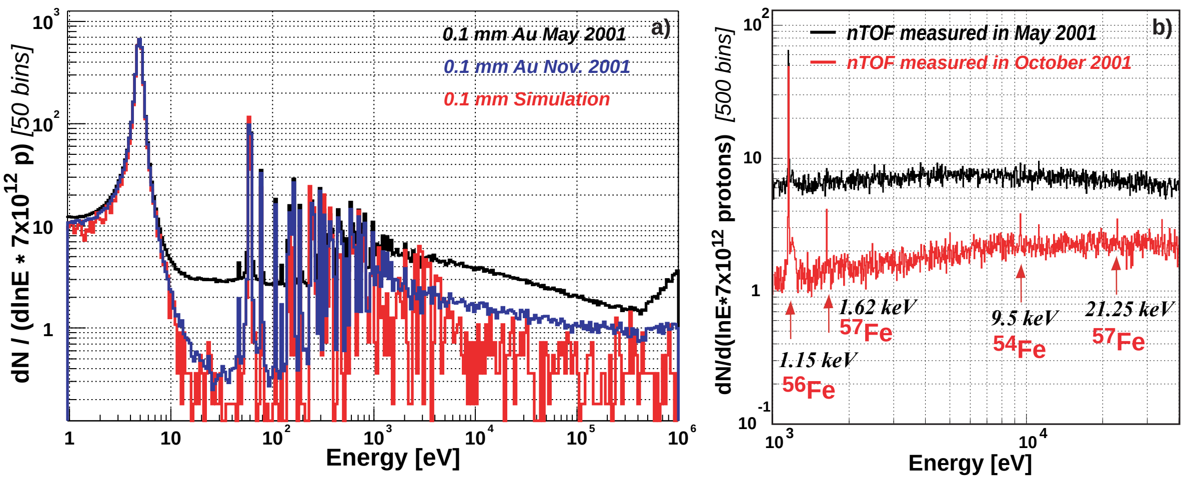

Figure 28. a) Count rate measured with a C_6D_6 detector for a 0.1-mm Au sample, **b)** with a 1.5-mm Fe sample. The raw neutron capture spectra obtained in the May/June campaign (black histogram) are compared with the results obtained after the installation of the 3.2 m iron wall in the secondary area. The simulation spectrum is also shown in the case of gold.

A more refined analysis is needed in order to evaluate the influence of the different background components on the measurements of capture cross sections for various isotopes. In particular, the application of the pulse height weighting technique is expected to produce a further improvement in the peak-to-valley ratio. This treatment considerably reduces the effect of soft in-beam γ rays scattered by the sample, which may currently account for a large fraction of the observed background at the sample position (see Section 3.2.4). This detailed analysis of the C_6D_6 data is in progress and will be presented in another technical note [5]. Finally, the effect of the 3 m iron shield on the background at small time-of-flights, in particular for the BaF_2 detectors, has still to be properly evaluated. Nevertheless, the results shown here indicate that a major improvement in the experimental conditions at n_TOF has been achieved through the installation of the 3.2 m iron wall.

4.3 TLD Measurements

After the 3.2 m wall installation, measurements were performed with a set of TLD detectors, which are sensitive to energy deposition, mainly from muons and high-energy γ's. The results are compared to the ones obtained in May 2001 in Figure 29.

The values are in μGy/h normalized to $4{\times}7{\times}10^{12}$ protons and to a 16.8 s cycle. The comparison of the results reported in the figure shows clearly the effect of the additional shielding (about a factor 30).

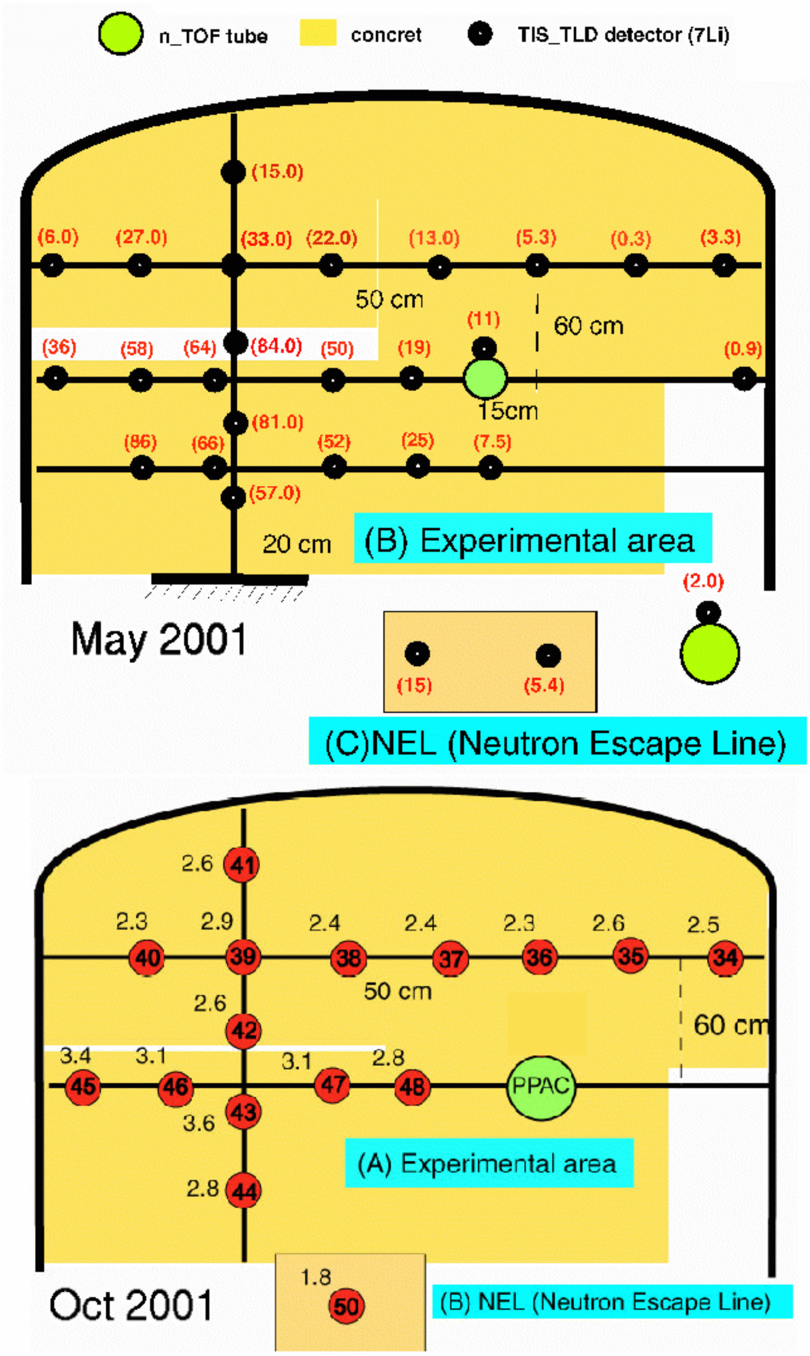

Figure 29. Results from TLDs (in µGy/h). Top figure: measurements done in May 2001; the values are indicated in parenthesis. Bottom figure: measurements done after the installation of the iron wall. The values are indicated above the TLD identification numbers.

4.4 Conclusions from the Second Phase of Measurements

After the installation of the iron wall the count rates measured with the ^{3}He counter were decreased by a factor 17 on the right side and a factor 9 on the left side, compared to the count rates obtained in the reference measurement.

By inserting the beam stopper, a reduction factor of about 30 was observed.

These results indicate that the neutron beam-related background is now half or more of the total background. Similarly, the sample-related background is now very important.

A synthetic comparative presentation of all results (first and second phase) is given in Figure 30.

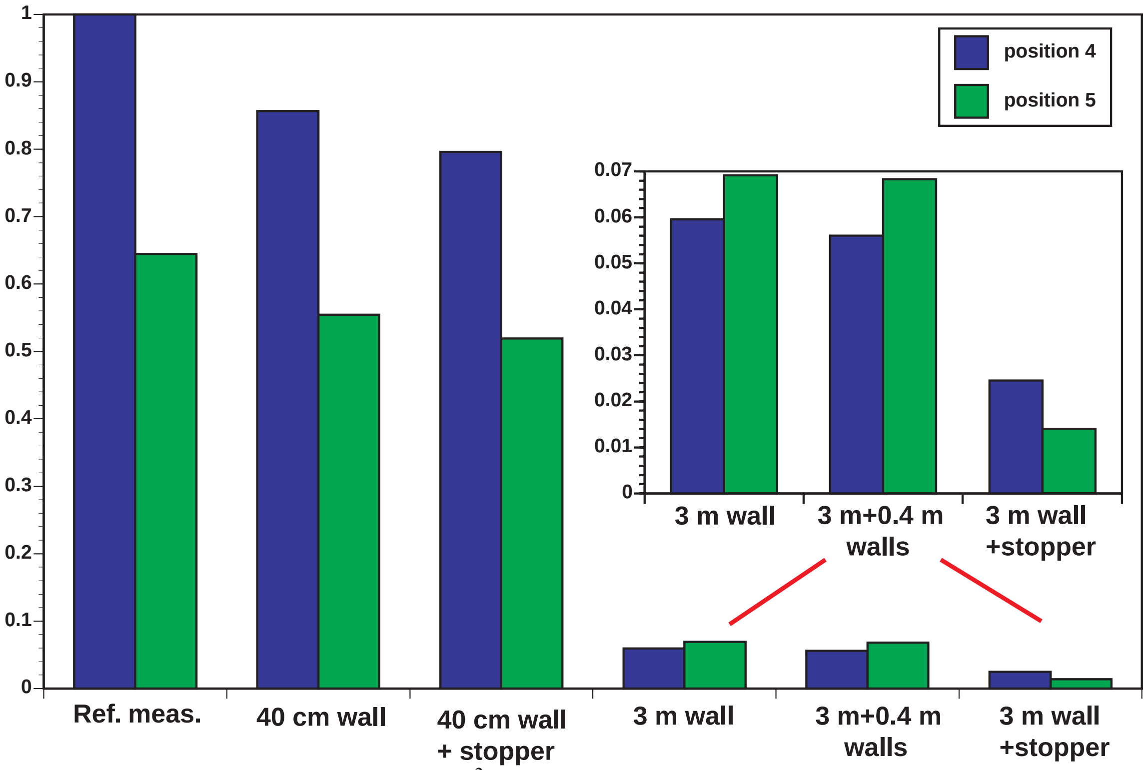

Figure 30. Total count rates of ^{3}He detector in positions 4 and 5 (normalized to the reference measurement in position 4) during the different measurements performed as described in the text.

The results obtained with the C_6D_6 are in agreement with those obtained with the ^{3}He. With the beam stopper the background reduction factor is of about 40. The C_6D_6 measurements confirm the importance of the beam-related background.

5. CONCLUSIONS

The study of the background in the n_TOF measuring station has been undertaken by means of both simulations and measurements.

The measurements confirmed the results from the simulations concerning the mechanism of the background production. Additional shielding was mounted in the n_TOF tunnel with characteristics determined by these studies and material availability.

As a result of the installation of the shielding, a strong background reduction was achieved.

The background related to the beam is now dominant in the experimental area. Scattering effects on the samples can also contribute significantly to the background depending on the mass used.

The component of the γ background coming from air activation was investigated. Through a sealing of the wall separating the measuring station from the secondary zone this component was strongly reduced.

Neutron-capture measurements with the Au sample show that the peak-to-ratio value for the Au neutron resonances has substantially improved.

However, measurements of isotopes with low capture cross-section or low-mass samples could require an additional improvement of the local background level.

An improvement in the shielding, together with the lining of the experimental area with borated polyethylene, could lead to a further reduction of the background.

ACKNOWLEDGEMENTS

We would like to thank Prof. C. Birattari from the University of Milano for kindly providing us the ^{3}He detector. The procurement of the iron by CERN, especially by M. Clément/SL, is greatly acknowledged.

References

[1] The n_TOF Collaboration, *Status Report*, CERN/INTC 2001-21, 2 August 2001.
[2] A. Ferrari, C. Rubbia, V. Vlachoudis, *A Comprehensive Study of the n_TOF Background*, n_TOF note 211009, SL-EET Note 2001-036.
[3] V. Vlachoudis, *A Multi-Purpose DAQ System Developed for the n_TOF Commissioning*, EET Internal Note 2001-03, 2001.
[4] V. Lacoste, L. Zanini, C. Borcea, E. Gonzalez, M. Heil, V. Vlachoudis, *Gamma Background Measurement in the n_TOF Experimental Area*, EET Int. note 2001-002.
[5] D. Cano-Ott *et al.*, *Detailed Analysis of the C_6D_6 Data from the n_TOF October 2001 Period after Installation of the Iron Shielding*, in preparation.

APPENDIX A. Time-Energy Relation

In Figure 31 the time-energy relation for a flight length of 186 m in vacuum is shown. This relation is valid for the neutron beam. The neutron energy scale was used in the case of the measurements with the C_6D_6 to indicate the energy regions affected by background events coming at a given time.

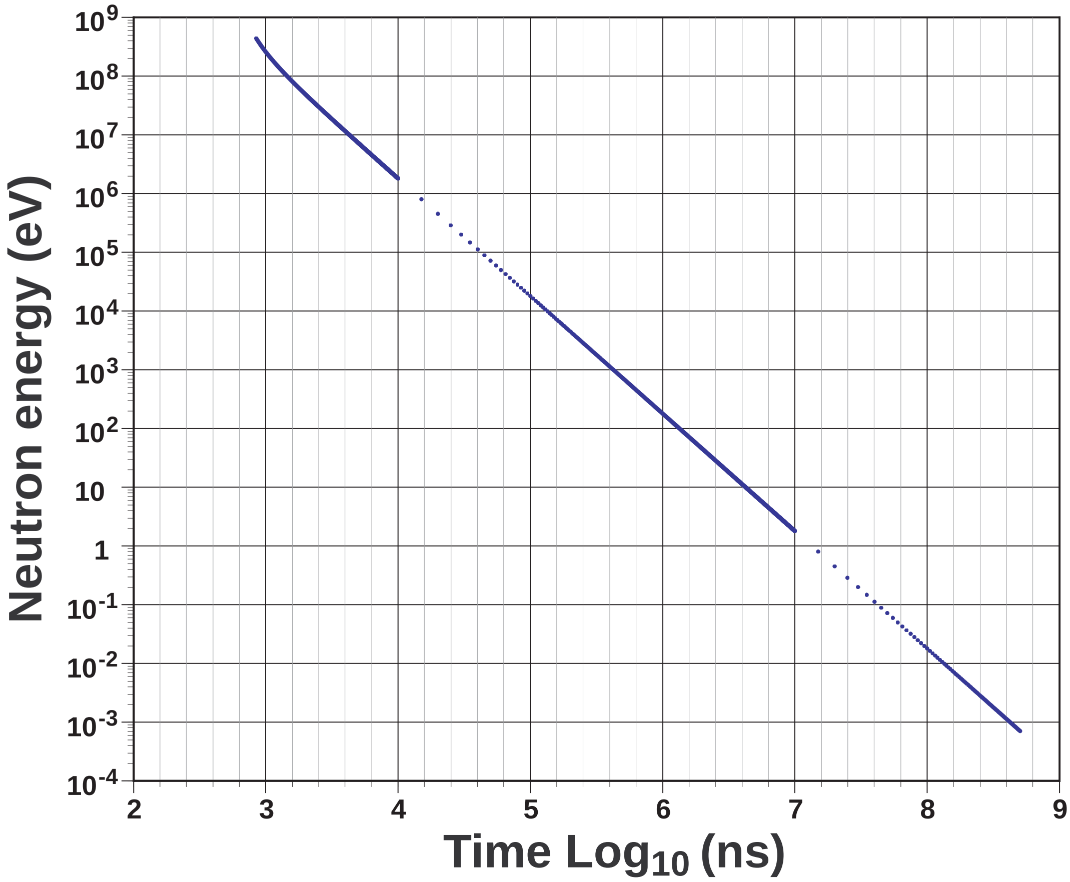

Figure 31. Correspondence between the time of an event and the neutron energy, for a flight distance of 186 m.

APPENDIX B. List of ^{3}He runs analyzed

Table 4. List of the ^{3}He runs analyzed in different measurements and configurations.

Position #	Small poly	Small poly + Cd	Big poly
BEFORE INSTALLING THE SHIELDING			
MEASUREMENT #0: REFERENCE MEASUREMENT			
1	851	843	
2	850	849	
3	852	844	
4	869,884,887	883	895
5	902	882	896,897
MEASUREMENT #1: 40 cm WALL			
4	905,913	906,914	
5	911	915	917
MEASUREMENT #2: 40 cm WALL + BEAM STOPPER			
4	925,928	929	
5	930		
AFTER INSTALLING THE SHIELDING			
MEASUREMENT #3: IRON WALL+ BEAM STOPPER			
4	946	942	
5	952	950	
MEASUREMENT #4: IRON WALL, BEAM STOPPER OUT			
4	954		
5	955		
MEASUREMENT #5: IRON WALL+40 cm WALL, BEAM STOPPER OUT			
4	969		
5	965		